NASA-CR-189,536

NASA-CR-189536
19920008781

IONIZING RADIATION EXPOSURE OF LDEF

Edited by

E. V. Benton
University of San Francisco, U.S.A.

W. Heinrich
University of Siegen, F.R.G.

(NASA-CR-189536) IONIZING RADIATION EXPOSURE OF LDEF (San Francisco Univ.) 66 p
CSCL 22B
N92-18023
Unclas
G3/18 0064250

(LDEF Pre-Recovery Estimates)

August 1990

USF-TR-77

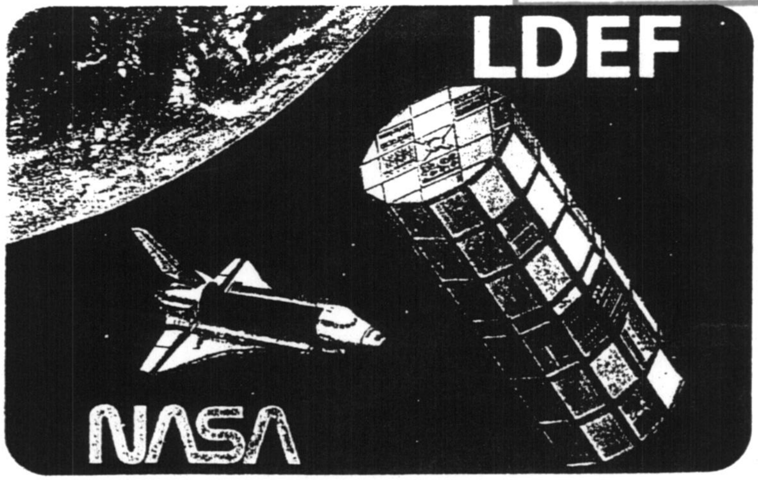

```
   SCREEN IMAGE   USER=*EBB       SESSION=T20BR08     4/15/92-09:51:33-AM

          DISPLAY 92N18023/2
        92N18023*#   ISSUE 9   PAGE 1410   CATEGORY 18   RPT#: NASA-CR-189536 NAS
        1.26:189536 USF-TR-77   CNT#: NAG8-138   90/08/00  66 PAGES   UNCLASSIFIED
        DOCUMENT
  UTTL: Ionizing radiation exposure of LDEF
  AUTH: A/BENTON, E. V.;  B/HEINRICH, W.   PAA: B/(Siegen Univ.,, Germany, F.R. )
        PAT: A/ed.;  B/ed.
  CORP: San Francisco Univ., CA.
  SAP:  Avail: NTIS HC/MF A04
  CIO:  UNITED STATES
  MAJS: /*CIRCULAR ORBITS/*DEPLOYMENT/*IONIZING RADIATION/*LONG DURATION EXPOSURE
        FACILITY/*PAYLOADS/*RADIATION DETECTORS/*RADIATION DOSAGE/*SPACE SHUTTLES
  MINS: / CONSTRUCTION/ DEFENSE PROGRAM/ PROPULSION/ SPACE MISSIONS/ SPACE STATION
        FREEDOM/ TRAYS/ UNIVERSITIES
  ABA:  Author
  ABS:  The Long Duration Exposure Facility (LDEF) was launched into orbit by the
        Space Shuttle 'Challenger' mission 41C on 6 April 1984 and was deployed on
        8 April 1984. The original altitude of the circular orbit was 258.5
        nautical miles (479 km) with the orbital inclination being 28.5 degrees.
        The 21,500 lb NASA Langley Research Center satellite, having dimensions of
        some 30x14 ft was one of the largest payloads ever deployed by the Space
        Shuttle. LDEF carried 57 major experiments and remained in orbit five
        years and nine months (completing 32,422 orbits). It was retrieved by the
   ENTER:                                                                    MORE
```

```
SCREEN IMAGE   USER=*EBB        SESSION=T20BR08      4/15/92-09:51:56-AM

      DISPLAY 92N18023/2
 Shuttle 'Columbia' on January 11, 1990. By that time, the LDEF orbit had
 decayed to the altitude of 175 nm (324 km). The experiments were mounted
 around the periphery of the LDEF on 86 trays and involved the
 representation of more than 200 investigators, 33 private companies, 21
 universities, seven NASA centers, nine Department of Defense laboratories
 and eight foreign countries. The experiments covered a wide range of
 disciplines including basic science, electronics, optics, materials,
 structures, power and propulsion. The data contained in the LDEF mission
 represents an invaluable asset and one which is not likely to be
 duplicated in the foreseeable future. The data and the subsequent
 knowledge which will evolve from the analysis of the LDEF experiments will
 have a very important bearing on the design and construction of the Space
 Station Freedom and indeed on other long-term, near-earth orbital space
 missions. A list of the LDEF experiments according to experiment category
 and sponsor is given, as well as a list of experiments containing
 radiation detectors on LDEF including the LDEF experiment number, the
 title of the experiment, the principal investigator, and the type of
 radiation detectors carried by the specific experiment.



ENTER:
```

IONIZING RADIATION EXPOSURE OF LDEF*

TABLE OF CONTENTS

N92-18023 #

*Work partially supported by NASA Grant NAG8-138
NASA George C. Marshall Space Flight Center,
Marshall Space Flight Center, AL 35812

I. INTRODUCTION

I.1 Value of LDEF Experiments

The Long Duration Exposure Facility (LDEF) was launched into orbit by the Space Shuttle "Challenger" mission 41C on 6 April 1984 and was deployed on 8 April 1984. The original altitude of the circular orbit was 258.5 nautical miles (479 km) with the orbital inclination being 28.5°. The 21,500 lb NASA Langley Research Center satellite, having dimensions of some 30×14 ft was one of the largest payloads ever deployed by the Space Shuttle. LDEF carried 57 major experiments and remained in orbit five years and nine months (completing 32,422 orbits). It was retrieved by the Shuttle "Columbia" on January 11, 1990. By that time, the LDEF orbit had decayed to the altitude of 175 nm (324 km) (see Fig. I.1). The experiments were mounted around the periphery of the LDEF on 86 trays and involved the representation of more than 200 investigators, 33 private companies, 21 universities, seven NASA centers, nine Department of Defense laboratories and eight foreign countries. The experiments covered a wide range of disciplines including basic science, electronics, optics, materials, structures, power and propulsion. The data contained in the LDEF mission represents an invaluable asset and one which is not likely to be duplicated in the foreseeable future. The data and the subsequent knowledge which will evolve from the analysis of the LDEF experiments will have a very important bearing on the design and construction of the Space Station Freedom and indeed on other long-term, near-earth orbital space missions.

I.2 List of LDEF Radiation Experiments

Table I.1 contains a list of the LDEF experiments according to experiment category and sponsor. The following two pages comprise a list of the experiments containing radiation detectors on LDEF including the LDEF experiment number, the title of the experiment, the principal investigator, and the type of radiation detectors carried by the specific experiment. For several experiments, the measurement of some aspect of the space radiation environment was the principal objective of the experiments. For others, the measurements were included to monitor the environment near a component which might exhibit some change due to the radiation. The large number of detectors at various locations around LDEF, and at various shielding depths, will allow a detailed comparison with calculated values from radiation environment models. This comparison will allow adjustment of the models and accurate extrapolation of the environments, to any point in LDEF, as well as other spacecraft.

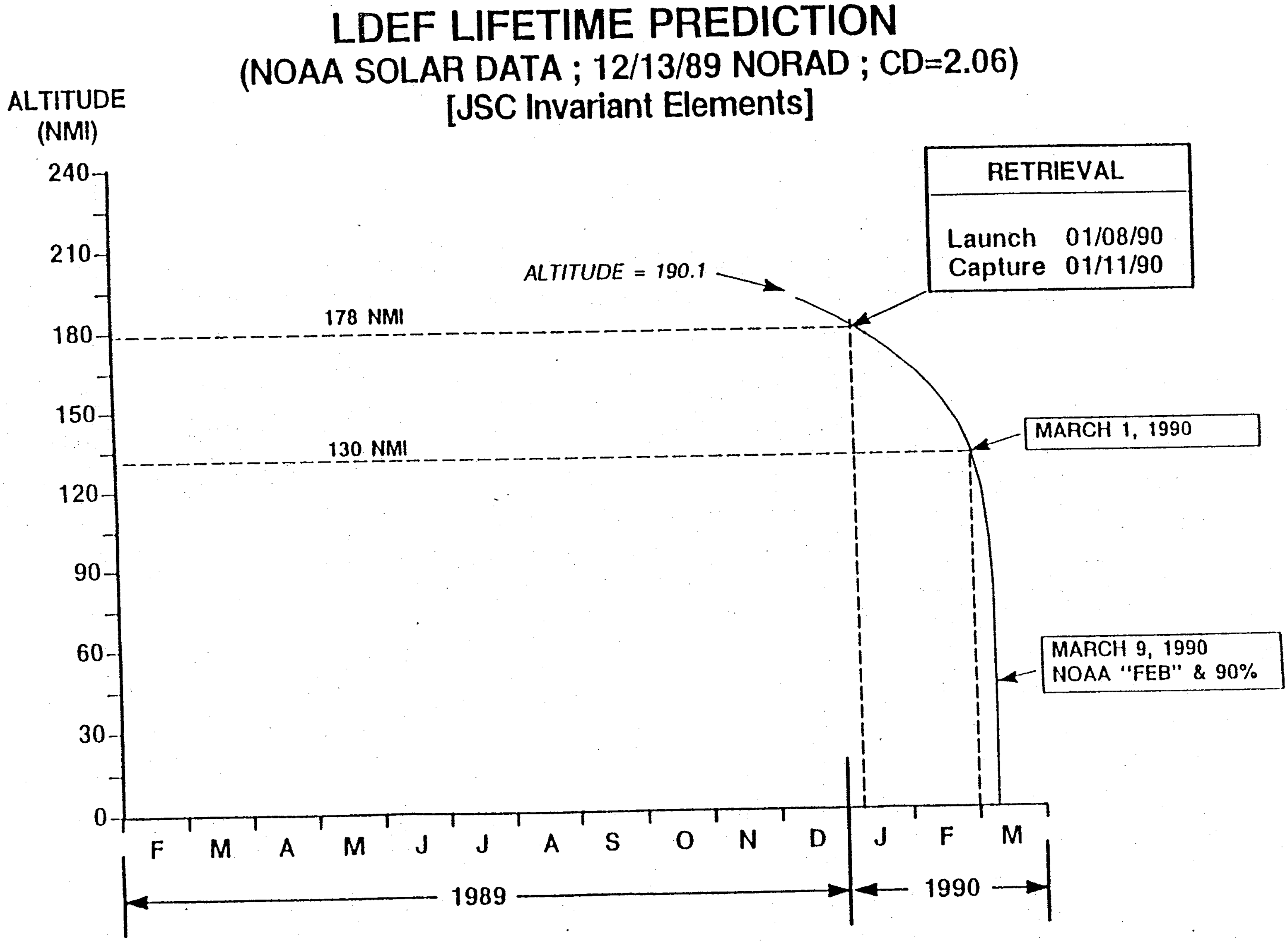

LDEF LIFETIME PREDICTION
(NOAA SOLAR DATA ; 12/13/89 NORAD ; CD=2.06)
[JSC Invariant Elements]

Figure I.1

TABLE I.1 List of LDEF Experiments According to Experiment Category and Sponsor

EXPERIMENTS CONTAINING RADIATION DETECTORS: PRINCIPAL CATEGORIES

ENVIRONMENT	DOSIMETRY/EFFECTS	ASTROPHYSICS	SPONSOR
P0004-1	P0004-1		NASA
P0004-2	P0004-2		NASA
P0006	P0006		NASA
M0001	M0001	M0001	DOD
M0002-1	M0002-1		DOD
M0002-2		M0002-2	FRG
M0003-12&17	M0003-12&17		DOD
M0004	M0004		DOD
A0015	A0015		FRG
A0138-7	A0138-7		FRANCE
A0114	A0114		NASA
A0178		A0178	IRELAND
ACTIVATION SUB-EXPERIMENT	ACTIVATION SUB-EXPERIMENT		NASA
FULL-LDEF ACTIVATION	FULL LDEF ACTIVATION		DOD

RADIATION DETECTORS
CARRIED IN FOLLOWING LDEF EXPERIMENTS

P0004-1	"SEEDS IN SPACE EXPERIMENT", GEORGE B. PARK JR. [F2] {TLD,PNTD} (P146)
P0004-2	"SPACE EXPOSED EXPERIMENT DEVELOPED FOR STUDENTS (SEEDS)", J.G. MARLINS [F2] {TLD, PNTD} (P148)
P0006	"LINEAR ENERGY TRANSFER SPECTRUM MEASUREMENT EXPERIMENT", E.V. BENTON [F2] {TLD, PNTD, FISSION FOILS, ACTIVATION METALS} (P115)
M0001	"HEAVY IONS IN SPACE", J.H. ADAMS, [H12]) {PNTD, ACTIVATION METALS} (P105)
M0002-1	"TRAPPED PROTON ENERGY SPECTRUM DETERMINATION", GARY MULLIN, [D3, D9, G12] {PNTD, TLD(G12), MICROSPHERES (12), ACTIVATION METALS} (P109)
M0002-2	"MEASUREMENT OF HEAVY COSMIC RAY NUCLEI ON LDEF", R. BEAUJEAN - [E6] {PNTD} (P113)
M0003-12-17	"SPACE ENVIRONMENT EFFECTS ON SPACECRAFT MATERIALS", SAM IMAMOTO [D3,D4,D8,D9] {TLD} (P45)
M0004	"SPACE ENVIRONMENTAL EFFECTS ON FIBER OPTICS SYSTEMS" - E.W. TAYLOR [F8] {TLD PNTD} (P185)

A0015	"FREE FLYER BIOSTACK EXPERIMENT", H. BÜCKER, [C2] {PNTD, FISSION FOILS, AgCl} (P139)
A0138-7	"OPTICAL FIBERS AND COMPONENTS EXPERIMENT," J. BOURRIEU [B3] {TLD} (P165)
A0114	"INTERACTION OF ATOMIC OXYGEN WITH SOLID SURFACES AT ORBITAL ALTITUDES", J.C. GREGORY [C2, C9] {ACTIVATION METALS} (P14)
A0178	"A HIGH RESOLUTION STUDY OF ULTRAHEAVY COSMIC RAY NUCLEI", D. O'SULLIVAN [A2, A4, A10, B5, B7, C5, C6, C8, C11, D1, D5, D7, D11, E2, E10, F4] {PNTD} (P101)
-----	"ACTIVATION SUB-EXPERIMENTS", G.J. FISHMAN [CARRIED IN P0006(F2), M0001(H12), M0002-1(D3,D9,G12), A0114(C3,C9)] {ACTIVATION METALS (CO, IN, NI, TA, V)} (SEE LDEF INDUCED RADIOACTIVITY ANALYSIS PLAN)
-----	"ACTIVATION OF LDEF STRUCTURE AND EXPERIMENT MATERIALS" LDEF IRSIG [MANY LOCATIONS] {MANY MATERIALS} (SEE LDEF INDUCED RADIOACTIVITY ANALYSIS PLAN) AND LIST OF IRSIG INTERESTS IN OTHER EXPERIMENTS

NOTE: [LDEF TRAY] {DETECTORS} (PAGE IN NASA SP-473)

TLD - THERMOLUMINESCENT DETECTORS - TOTAL ABSORBED DOSE

PNTD- PASSIVE NUCLEAR TRACK DETECTORS - MEASURE HEAVY IONS AND LINEAR ENERGY TRANSFER (LET) SPECTRA

The following page contains information on the various experiments, the principal detector used in each experiment and the end-point of the measurement.

LDEF IRSIG TAP 10/24/89

RADIATION DETECTORS ON LDEF

	TLD'S	PNTD'S	Activated Materials	Fission Foils	Other Detectors
	Absorbed Dose (Rads)	Heavy Ion Fluence & LET Spectra	Proton & Neutron Fluence	Neutrons & Spectra	
P0004-1	X	X			
P0004-2	X	X			
P0006	X	X	X	X	
M0001		X	X		
M0002-1	X	X	X		Microsphere
M0002-2		X	X		
M0003-12	X				
M0003-17	X				
M0004	X	X			
M0006	X				
A0015	X	X		X	Agcℓ
A0138-7	X		X		
A0114-1			X		
A0114-2			X		
A0178		X			
LDEF Structure & Experiments			X		

The following four pages show an unfolded map of the LDEF trays showing the different locations of the various experiments together with the designation of the "leading" and "trailing" edges, and the "space" and "Earth" ends of the LDEF spacecraft. The four pages show the distribution of the various detector types, including: thermoluminescent detectors (TLDs), plastic nuclear track detectors (PNTDs), activation foils, and the PNTDs used in the Ultra-Heavy Ion Fluence experiment.

Thermoluminescent Dosimeters (TLD) Absorbed Dose

5-11480-0-309

Bay / Row	A	B	C	D	E	F
1						
2			M0006			P0004 P0006
3		A0138				
4				M0003		
5						
6						
7						
8				M0003		M0004
9						
10						
11						
12						

Trailing Edge → 3

Leading Edge → 9

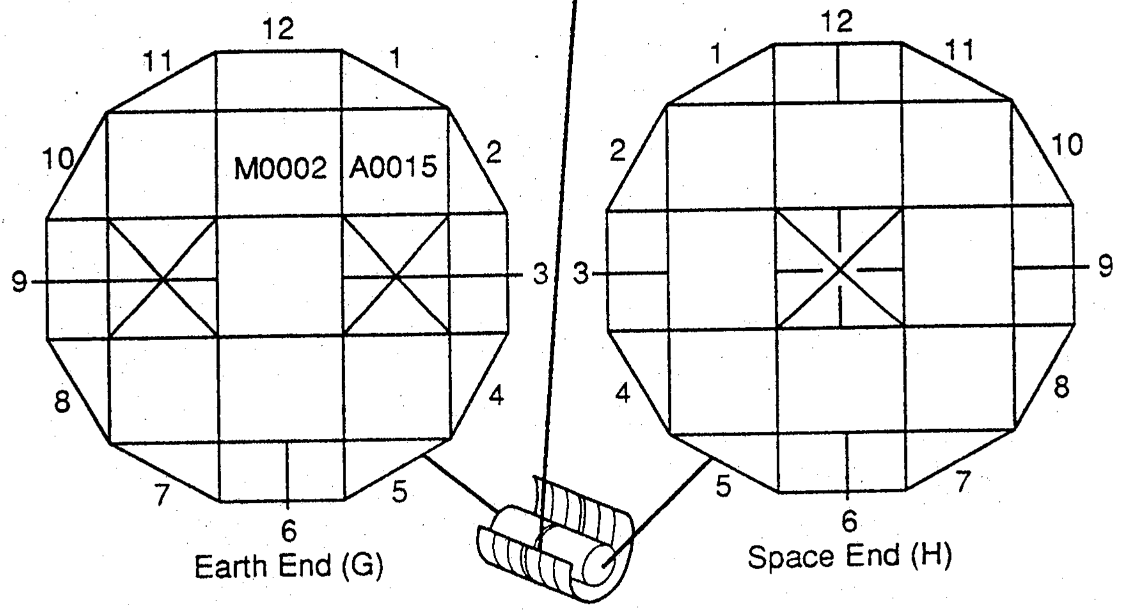

Passive Nuclear Track Detectors (PNTD)
LET Spectra, Heavy Ion Fluence

5-11479-0-309

Trailing Edge → Row 3

Leading Edge → Row 9

Bay / Row	A	B	C	D	E	F
1						
2			A0015			P0004 P0006
3				M0002		
4						
5						
6						
7						
8						M0004
9				M0002		
10						
11						
12						

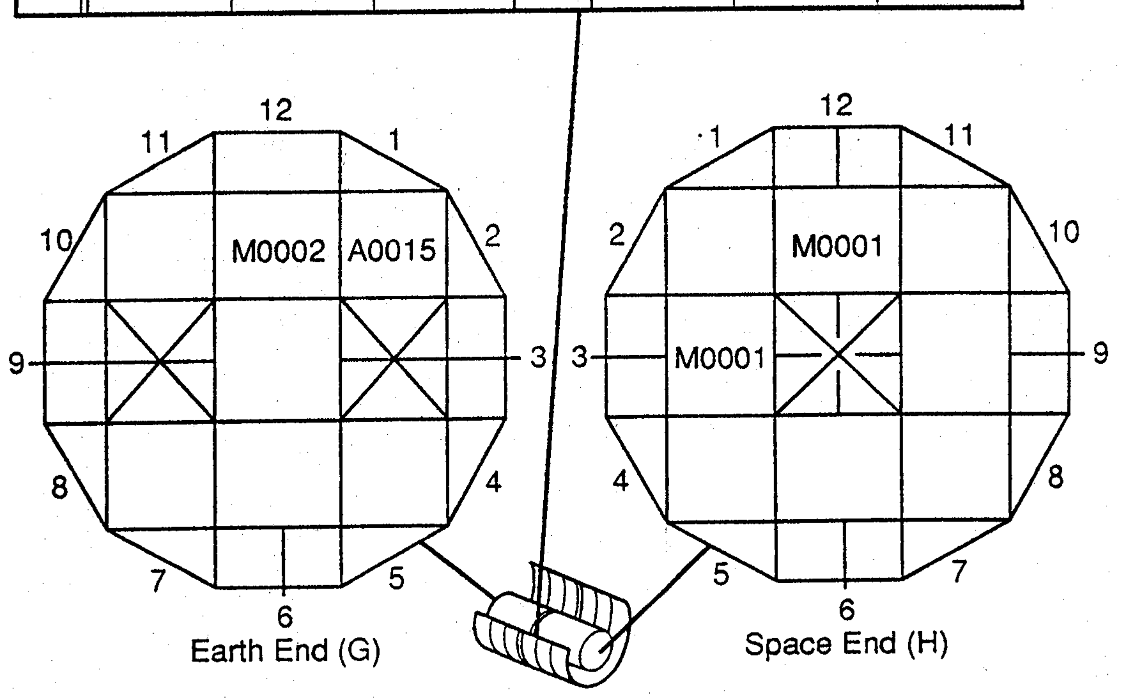

LDEF Sample Materials for Induced Radioactivity
400 Samples, 25 gm or Larger

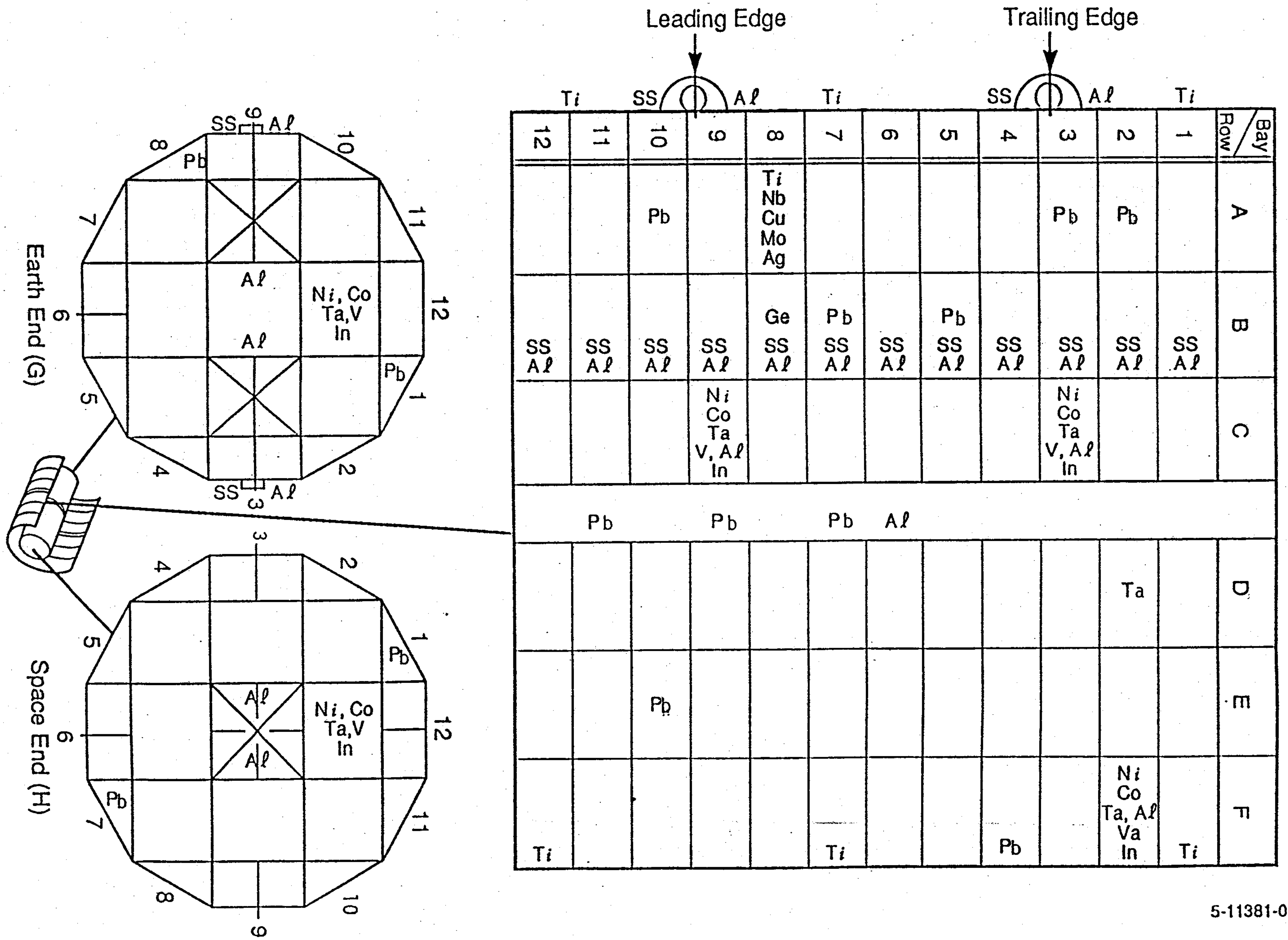

Bay / Row	A	B	C		D	E	F
1		SS Aℓ					Ti
2	Pb	SS Aℓ			Ta		Ni Co Ta, Aℓ Va In
3	Pb	SS Aℓ	Ni Co Ta V, Aℓ In				
4		SS Aℓ					Pb
5		Pb SS Aℓ					
6		SS Aℓ		Aℓ			
7		Pb SS Aℓ		Pb			Ti
8	Ti Nb Cu Mo Ag	Ge SS Aℓ					
9		SS Aℓ	Ni Co Ta V, Aℓ In	Pb			
10	Pb	SS Aℓ				Pb	
11		SS Aℓ		Pb			
12		SS Aℓ					Ti

5-11381-0-309

Passive Nuclear Track Detectors (PNTD)
Ultra Heavy Ion Fluence, Composition and Spectra

5-11481-0-309

Trailing Edge → Row 3

Leading Edge → Row 9

Bay / Row	A	B	C		D	E	F
1					A0178		
2	A0178					A0178	
3							
4	A0178	A0178					A0178
5			A0178		A0178		
6			A0178			M0002	
7		A0178			A0178		
8							
9							
10	A0178					A0178	
11			A0178		A0178		
12							

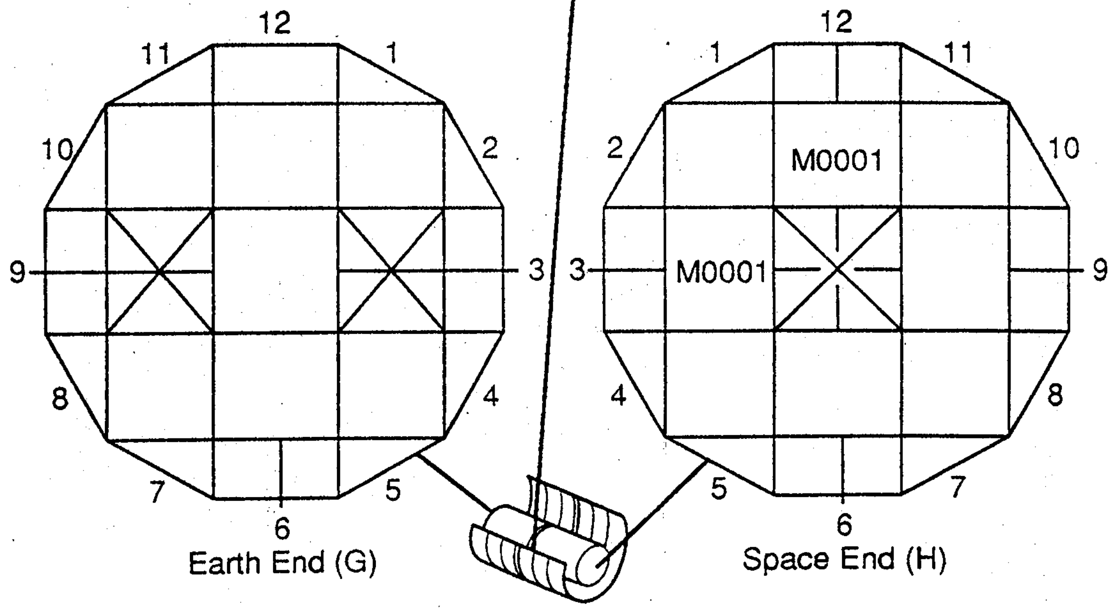

II. TRAPPED PARTICLES AND COSMIC RAYS

II.1 LDEF Environment

The LDEF spacecraft flew in a 28.5° inclination circular orbit with an altitude in the range from 175 to 258.5 nautical miles (324–479 km). It was gravity-gradient stabilized and oriented so that one side always pointed along the velocity vector. For this orbital altitude and inclination, two components contribute most of the penetrating charged particle radiation encountered–the geomagnetically trapped Van Allen protons and the galactic cosmic rays (GCR). Where shielding is less than 1.0 g/cm^2, geomagnetically trapped electrons make a significant contribution and dominate the surface absorbed dose. All three sources are strongly modulated by the earth's magnetic field. Also, under low shielding, "anomalous" cosmic rays can make an additional contribution to the total radiation exposure. Rare solar flares that produce energetic particles with energies well above 1 GeV could contribute a minor dose component at all shielding depths.

II.2 Trapped Particles

Under modest shielding on LDEF, over 95% of the radiation exposure will prove to be from trapped protons. Almost all the trapped flux is encountered in the region called the "South Atlantic Anomaly" (SAA), produced because the earth's magnetic field, though approximately dipolar, is not centered on the earth. The particles follow a helical path about a magnetic field line. As the field intensity increases, both the diameter and the pitch of the helix decrease until the pitch becomes zero. The point with zero pitch angle is called the mirror point and the center of the helical path is called the guiding center. From here the helix reverses direction and particles travel up the field line toward decreasing field intensity and away from the earth (see Fig. II.1).

In the SAA, almost all the protons observed are near their mirror points. Thus the flux is anisotropic with most of the flux arriving from a narrow band perpendicular to the local geomagnetic field direction (see Fig. II.2). Any protons there which are not nearly mirroring will travel deep into the atmosphere and be scattered or stopped by atmospheric interactions.

Atmospheric interactions also affect the proton angular distribution in another fashion. Protons that are observed traveling eastward are following guiding centers above the observation point and protons traveling westward are following guiding centers below the observation point. The gyroradius for energetic protons in the Anomaly is on the same order as the atmospheric density scale height. Thus westward traveling protons encounter a significantly denser atmosphere and are more likely to suffer atmospheric interactions and be lost. The resulting energy-dependent anisotropy is called the east-west effect.

Assuming that the mirror point density along a field line is proportional to the atmospheric density along the field line, Heckman and Nakano /1969/ showed that the pitch angle distribution is Gaussian with a standard deviation given by

$$\sigma = \sqrt{\frac{h_0}{K \sin I}} \tag{1}$$

where h_0 is the scale height, I is the magnetic dip angle and K is given by

$$K = \frac{4/3R}{\sin I(2 + \cos^2 I)} \tag{2}$$

where R is the dipolar radius.

Lenchek and Singer /1962/ give an expression for the east-west effect assuming, as observed, that the proton flux rises exponentially with altitude.

$$\frac{j_2}{j_1} = \exp\left(\frac{r \cos I(\cos\beta_2 - \cos\beta_1)}{h_0}\right) \tag{3}$$

where j_1 and j_2 are the fluxes seen from directions β_1 and β_2. The angles are measured relative to magnetic east. h_o is the scale height, r is the proton gyroradius given by

$$r = \frac{10^4 p}{cqB} \tag{4}$$

where r is in kilometers, p is momentum in MeV/c, c is the speed of light in km/s, q is the particle charge in electron charges, and B is the magnetic field intensity in Gauss. For typical values of the magnetic field parameters and atmospheric scale height in the Anomaly, the gyroradius for 50 MeV protons is 52 km and the ratio of the eastward traveling ($\beta_2 = 0°$) to the westward traveling ($\beta_1 = 180°$) flux is 3. At 400 MeV the values are 145 km and 22.

Given the omnidirectional flux from the Vette model /Sawyer and Vette, 1976/, the vector magnetic field /Stassinopoulos and Mead, 1972/, appropriate atmospheric scale height data /Johnson and Smith, 1965/, the pitch angle distribution from equation (1), and the east-west distribution from equation (3), an approximate vector proton flux distribution can be derived. Selecting a coordinate system with the z-axis point along B and its y-axis point toward magnetic east

$$j(E,\theta,\phi) = j_0(E)\frac{\exp\left(\frac{(\pi/2-\theta)^2}{2\sigma^2}\right)}{\sin\theta\sqrt{2\pi}\sigma\mathrm{erf}\left(\frac{\pi}{2\sqrt{2}\sigma}\right)}\frac{\exp\left(\frac{r\cos I\cos\beta(\theta,\phi)}{h_0}\right)}{\int_0^{2\pi}\exp\left(\frac{r\cos I\cos\beta(\theta,\phi)}{h_0}\right)d\phi} \tag{5}$$

where $j(E,\theta,\phi)$ is the vector flux in spherical coordinate direction (θ,ϕ) at energy E, $j_0(E)$ is the omnidirectional flux; Equation (5) yields the flux distribution in coordinates fixed to the magnetic field. Given the attitude of a spacecraft relative to the magnetic field, the distribution is then transformed by a rotation to the spacecraft coordinates.

For spacecraft stabilized in earth or magnetic coordinates in low-altitude orbits the anisotropic nature of the flux distribution is important if complex shielding geometries are being modeled. Using an omnidirectional flux distribution would introduce significant errors in the predictions at most locations.

Trapped electrons have energies of up to several MeV, but a mass 1/1840 that of protons, and magnetic gyroradii of at most a few meters. Thus they do not exhibit the east-west effect. They scatter significantly while being slowed in absorbers, reducing effects of directional properties. At the surface of LDEF the electrons will contribute the majority of the absorbed dose. The electron contribution decreases rapidly with shielding depth (see Section III, Fig. III.5).

II.3 Galactic Cosmic Rays (GCR)

The galactic cosmic rays consist mainly of the nuclei of the elements (hydrogen through uranium), with a broad energy spectrum and high average energy (~7 GeV). The geomagnetic field shields LDEF from nuclei below ~1 to 15 GeV, depending upon position in orbit. This reduces the GCR flux dose well below interplanetary space values. The LDEF dose contribution by GCR is predicted to be about 6 rad, decreasing more slowly with shielding depth than the trapped proton dose. The GCR absorbed dose is only ~1–3% of the trapped proton dose at typical shielding depths, but the importance of the GCR exposure is determined by additional considerations. These are due to the presence of heavy nuclei in the GCR, and the interactions of the GCR which produce more secondary particles and subsequent phenomena than the lower energy trapped protons. In the discussion of linear energy transfer (LET) spectra (Section IV) and secondary particles (Section V), the regions of the spectra and other effects dominated by GCR are described. Because of their high LETs, they have a significant influence on the LET spectra and hence on the rem dose, as well as being a major contributor to the electronic "single event upsets" (SEU) effects.

The GCR particles bombard the earth isotropically and consist of nuclei of all the elements of the periodic table spanning some 14 decades in energy (see Figs. II.3–II.6). The GCR composition in the vicinity of earth consists of ~98% nuclei and ~2% electrons and positrons. The nuclei consist of elements of the entire periodic table with about 87% hydrogen, ~12% helium and ~1% heavier nuclei /Simpson, 1983/. The particles are accelerated to a power law spectrum $dN/dE \propto E^{\approx -2.5}$ by processes within the galaxy to energies of at least 10^{15} electron volts. Above 10^{15} eV, the spectrum steepens to $dN/dE \propto E^{-3.1}$, indicating other processes and perhaps extra-galactic particles are involved up to 10^{20} electron volts. In the interplanetary space, the low energy solar wind particles carry associated magnetic fields that reduce the flux of low energy GCR (below a few GeV) and prevent those below ~100 MeV from reaching the earth's vicinity. The characteristic eleven-year cycle of solar activity "modulates" this behavior with maximum GCR flux occurring at solar minimum with a fluence rate of about 4 particles $cm^{-2}s^{-1}$ near earth. At solar maximum, this is reduced to ~2 $cm^{-2}s^{-1}$. The earth's magnetic field further reduces the GCR flux, except near the magnetic poles, where the interplanetary flux can penetrate without crossing field lines. In the LDEF orbit (28.5°, ~400 km), the "geomagnetic cut-off" for GCR varies from ~1 GeV/nucleon to ~10 GeV/nucleon at various orbital positions /Shea and Smart, 1975/. The average flux of GCR in LDEF is approximately 10^{-1} particles $cm^{-2}s^{-1}$. Thus the GCR dose in LDEF will be only a few percent of the interplanetary space values. Since the dose is proportional to atomic number Z, squared (see Fig. II.6), the absorbed dose from GCRs is dominated by the heavy nuclei.[1]

II.4 Solar Particle Events (SPE)

SPEs are relatively short-term (hours or days) periods during which large emissions of energetic charged particles (protons, helium and heavier ions) occur in space as the result of events on the sun. Large solar flares are a major source of SPEs where the larger fluences, near earth, are greater than ~ 10^{10} protons/cm^2 with energies greater than ~10 MeV (the August 1972 event, for example). Not all solar flares produce SPEs that are detectable near the earth (see Fig. II.7), and the duration and intensities of the events can vary widely (see Figs. II.8, II.9).

Since the LDEF orbit with inclination of 28.5° has a minimum geomagnetic cutoff of ~1 GeV, it is expected that even though some solar flare particles may have high enough energy to reach the spacecraft, the contribution to the dose is expected to be small. However, it was recently reported that the second half of 1989 was the most prolific period of relativistic particle production by the sun since continuous monitoring was begun in 1957, and that some 1989 events were among the largest bursts of particles observed throughout the last three solar cycles /Mathews and Venkatesan, 1990/. This increased activity is one of several indications that the levels of solar activity have been increasing gradually over the past 400 years. These changes are, apparently, the result of another solar cycle with a time-scale of several hundred years /Schatten, 1990/.

II.5 Anomalous Cosmic Rays

In situations involving little shielding, the anomalous component of cosmic rays can influence the LET spectra and the absorbed dose. The anomalous component of the energetic charged particle environment appears to originate when atoms from the interplanetary or interstellar media are first ionized by solar ultraviolet and then accelerated by the shock waves at heliopause. They consist of heavy ions, at least through oxygen, and perhaps protons, in the energy range of from ~1 to 40 MeV/nucleon. They appear to be singly ionized. This

---

[1] Even though iron abundance is only about one tenth that of carbon or oxygen, when converted to equivalent dose with the use of quality factors, the iron nuclei dominate.

component is strongly influenced by solar modulation and therefore is not always significant in the vicinity of the earth. These low energy ions have high specific ionization (dE/dx), and therefore influence the higher portion of the LET spectra at their shielding depths /Adams *et al.*, 1981, 1983a; Vahia and Biswas, 1983/.

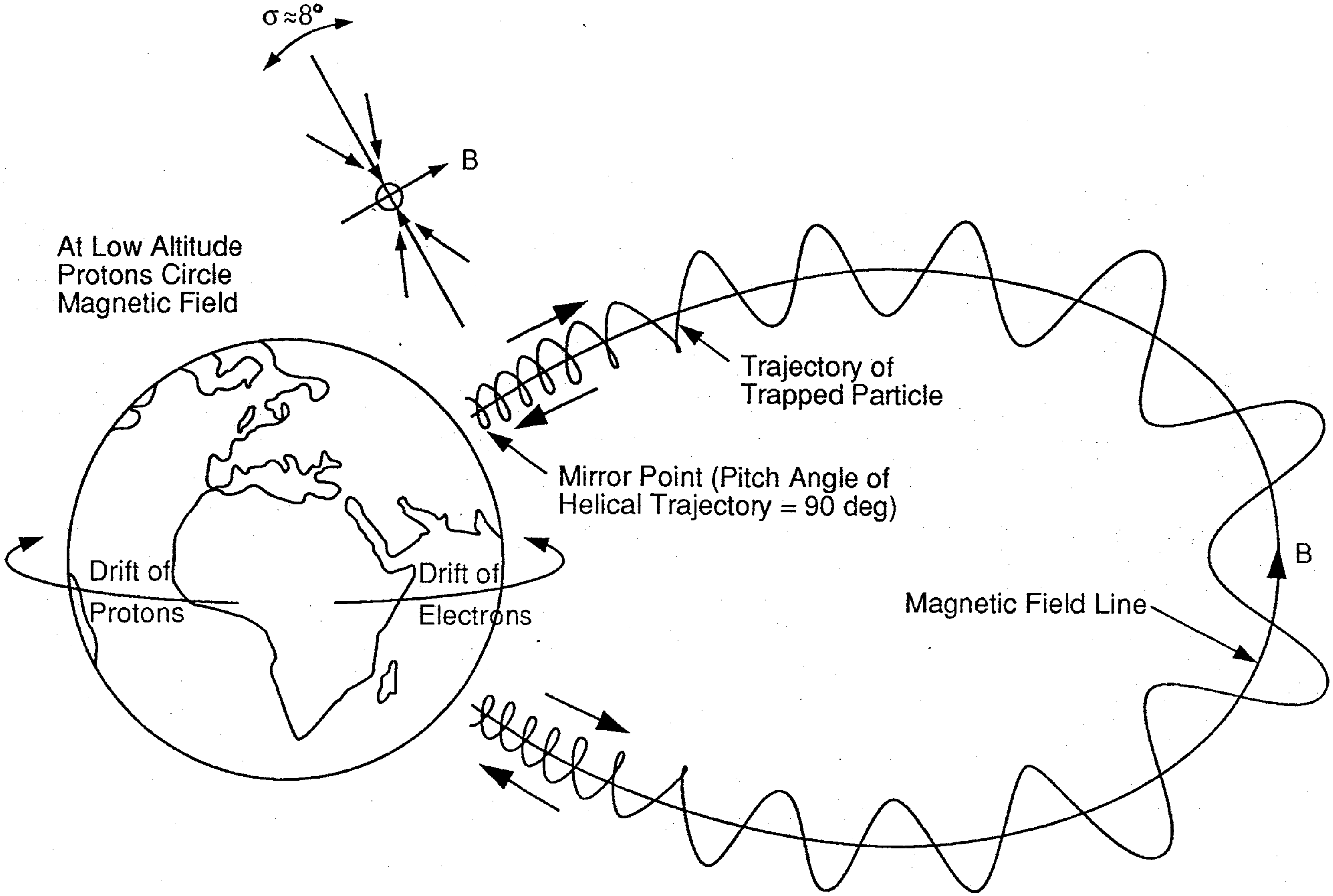

Fig. II.1 Path of trapped charged particles in the geomagnetic field (B) /Watts et al., 1989/.

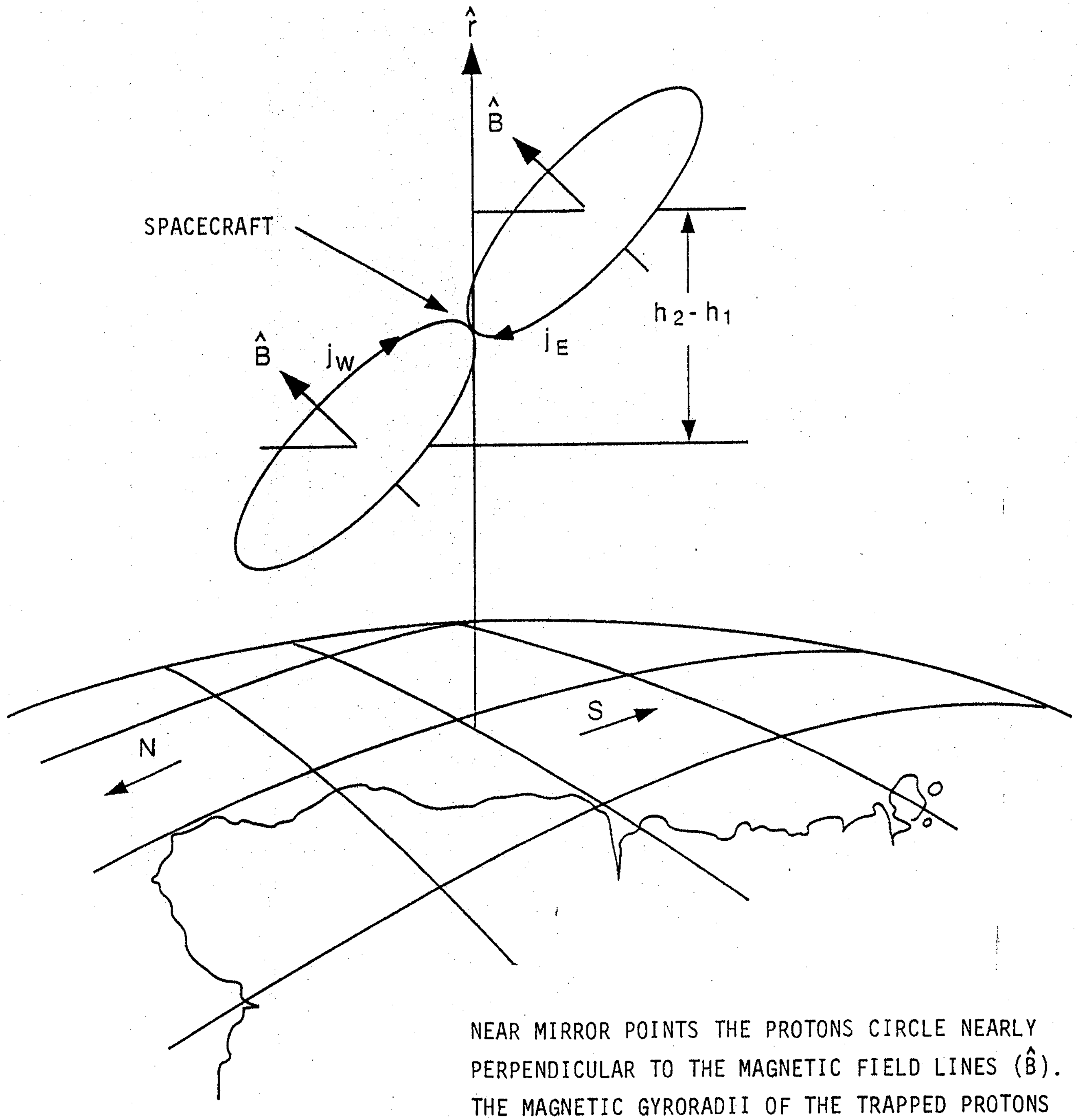

NEAR MIRROR POINTS THE PROTONS CIRCLE NEARLY PERPENDICULAR TO THE MAGNETIC FIELD LINES ($\hat{B}$). THE MAGNETIC GYRORADII OF THE TRAPPED PROTONS ARE CLOSE TO THE ATMOSPHERIC SCALE HEIGHT.

FIG. II.2 East-west effect coordinates.
/Watts et al., 1989./

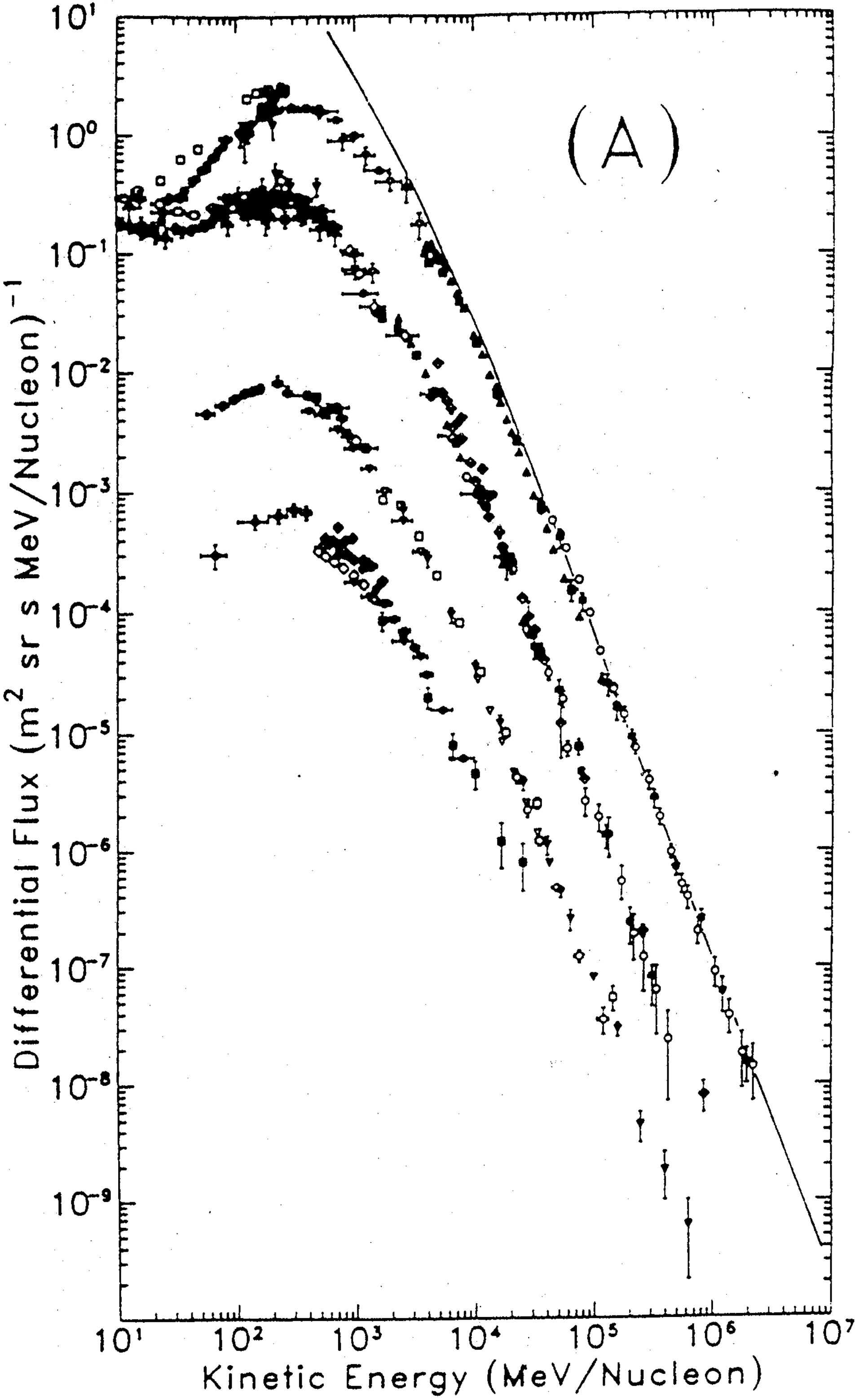

Fig. II.3 Energy spectra of galactic protons, helium ions, carbon ions, and iron ions respectively (from top to bottom) *at solar minimum* /Simpson, 1983/.

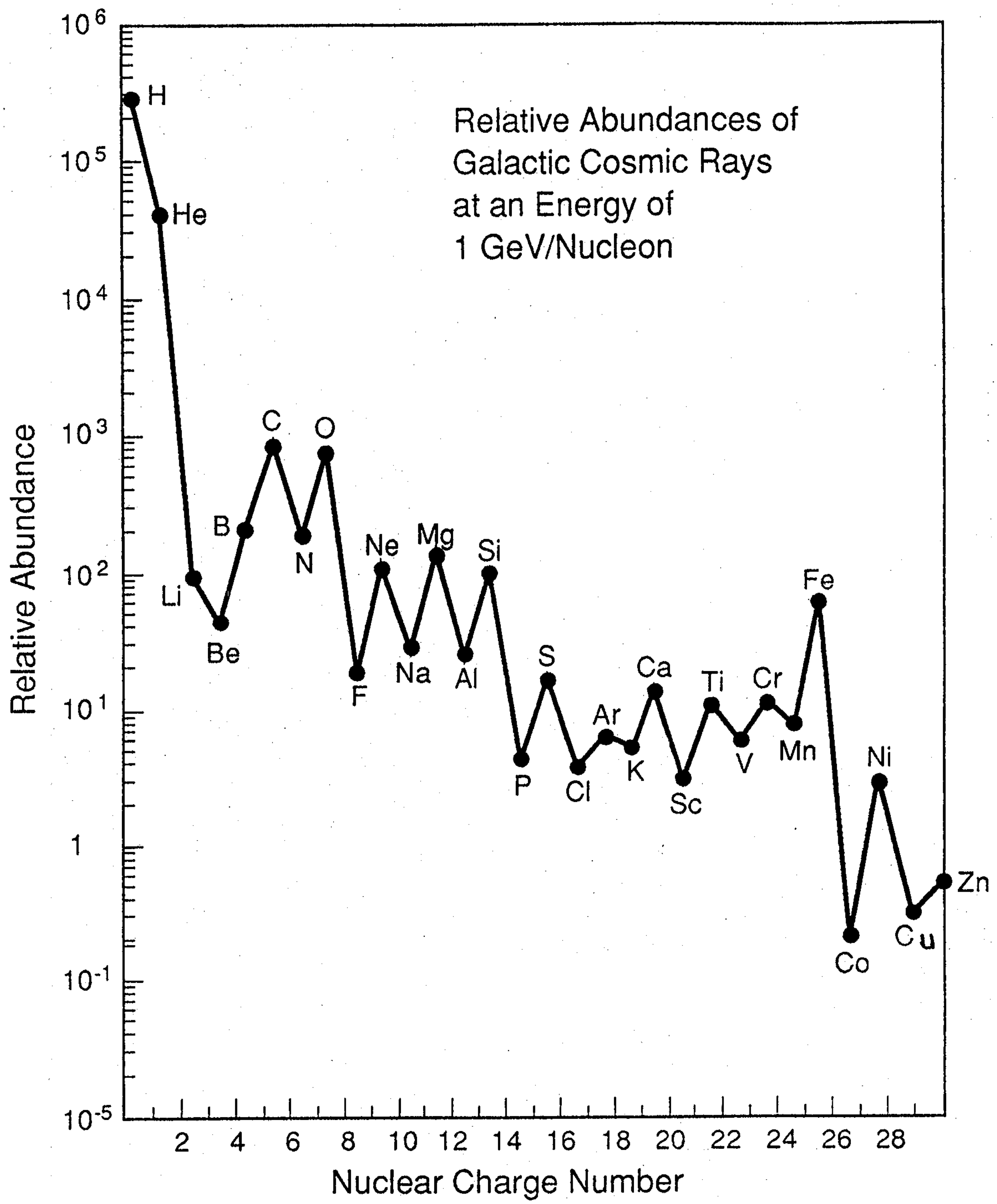

Fig. II.4 The measured abundances of the elements relative to silicon (≡ 100) in the galactic cosmic radiation. /Adapted from Simpson, 1983./

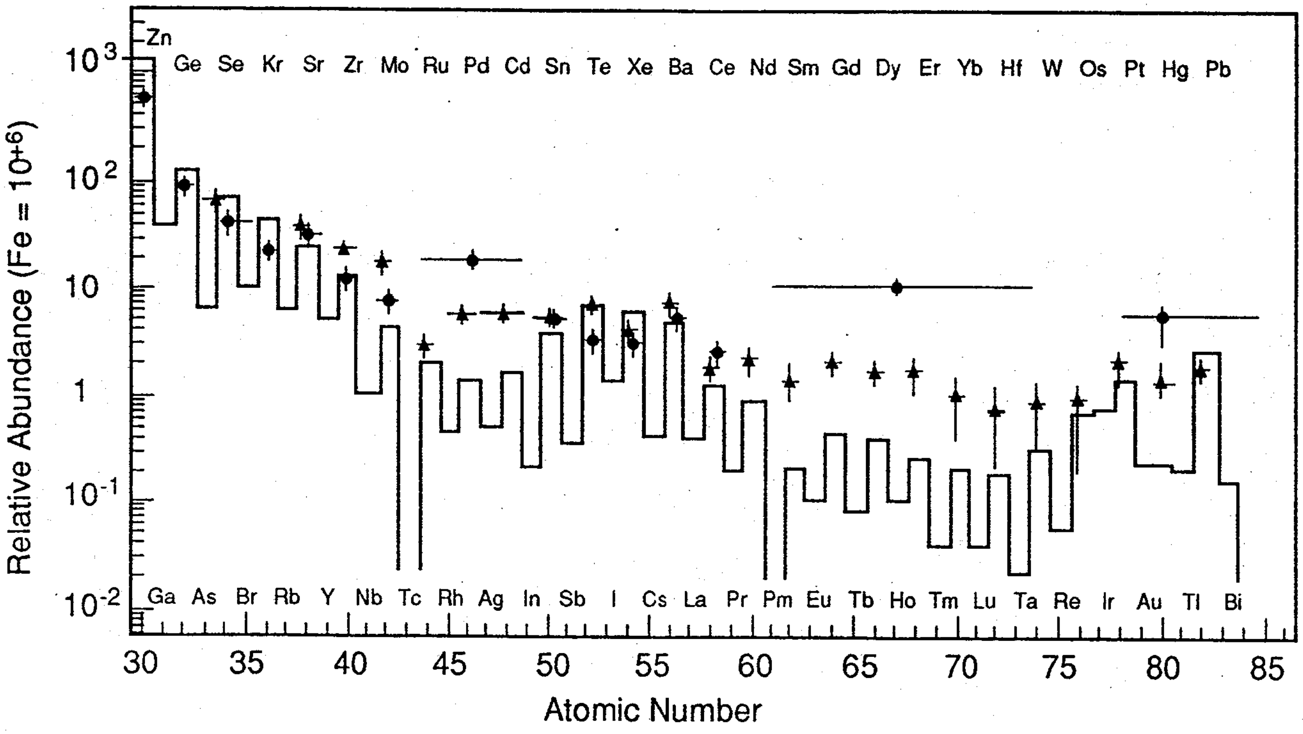

Fig. II.5 The relative abundances of galactic cosmic ray nuclei from atomic number 30 to 83. The data points are from the HEAO-C3 instrument /Binns et al., 1981/. The histogram shows solar system abundances as compiled by Cameron /1982/. Not shown here are the two thorium-uranium nuclei measured by HEAO-C3 in an 8 m^2-yr exposure. (This figure adapted from Wefel /1988/).

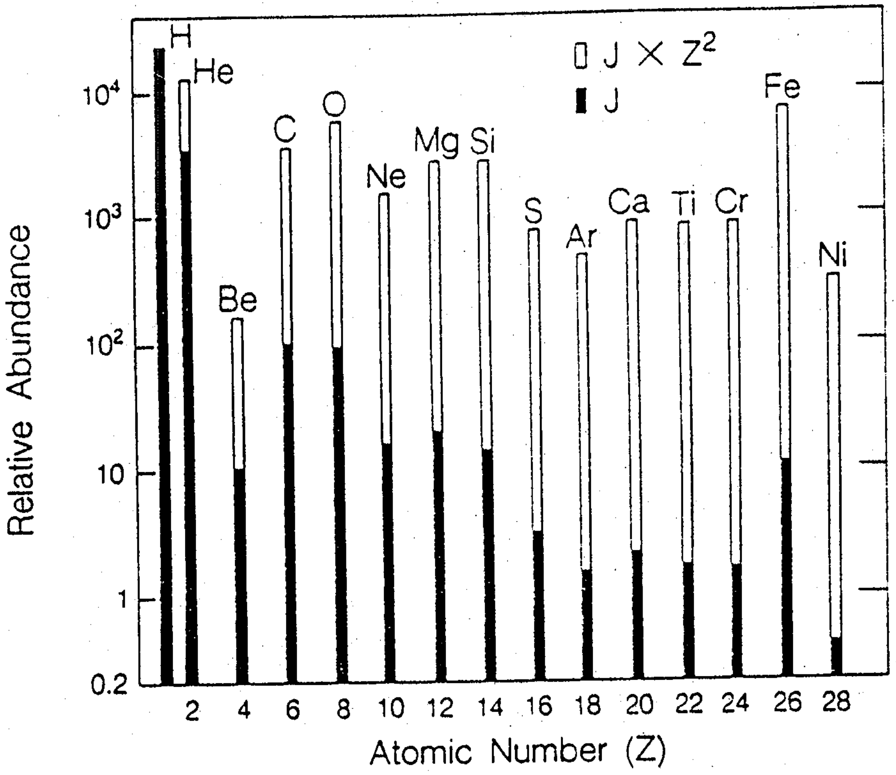

Fig. II.6 Histogram showing the relative abundances of the even-numbered galactic cosmic ray (GCR) nuclei (solid bars) compared to their abundances weighted by the square of the particle's charge to give a measure of the "ionizing power" of each element (open bars) /Wefel, 1974/.

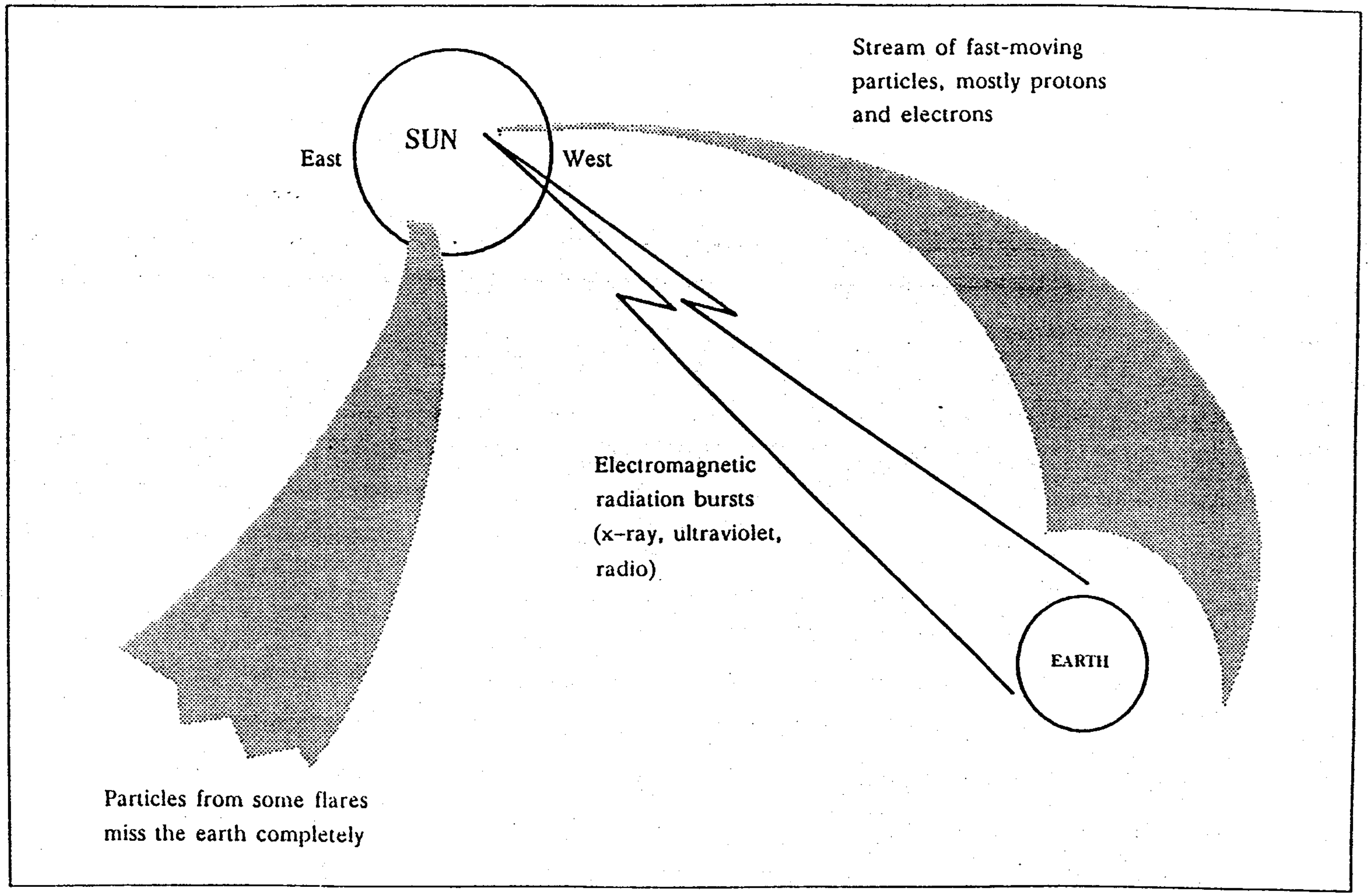

Fig. II.7 Energetic particles from solar flares generally follow spiral paths defined by the interplanetary magnetic field. Particles from active regions near the west limb will usually arrive at earth, those on the east may not. Electromagnetic emission travels line-of-sight /Wagner, 1987/.

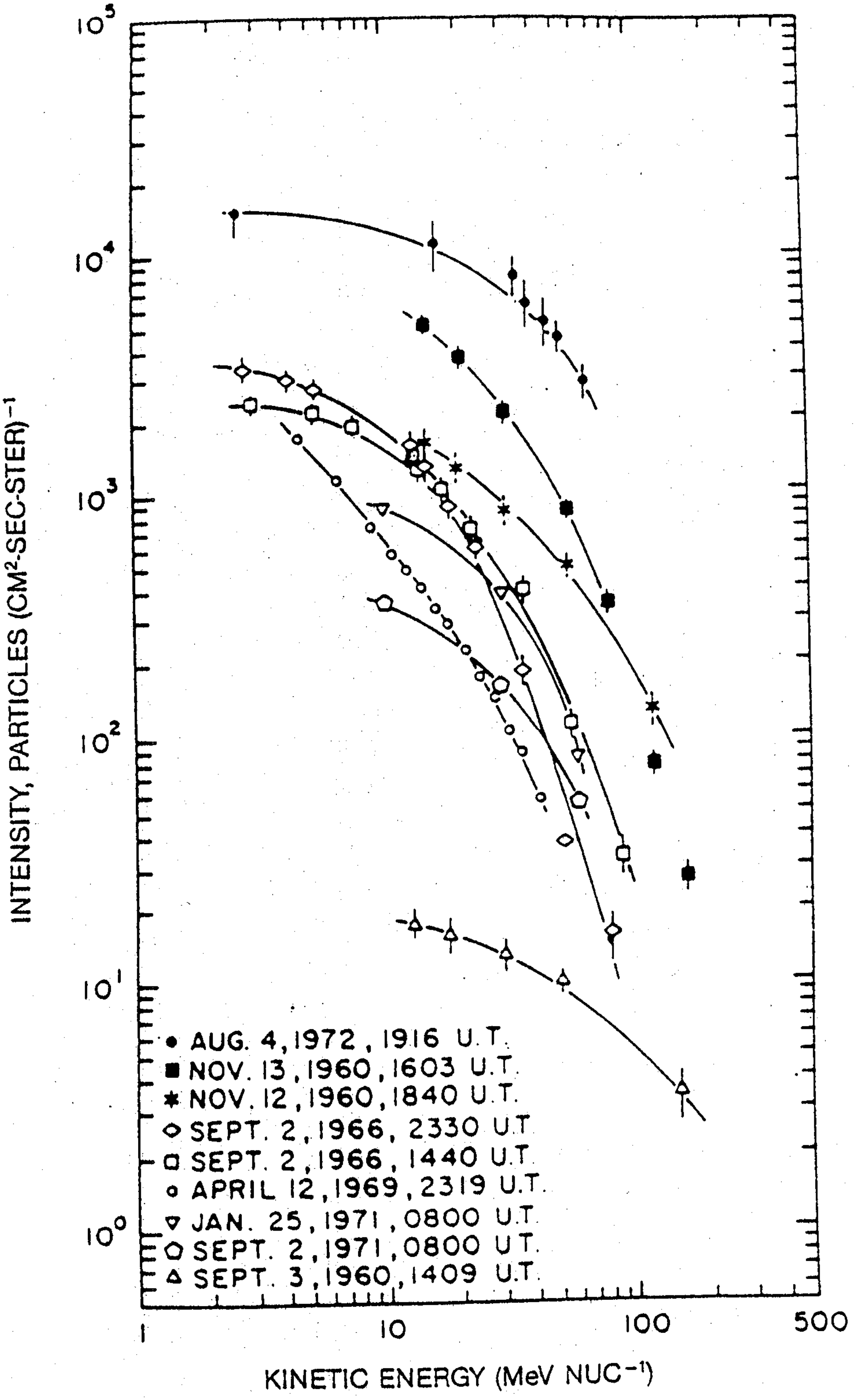

Fig. II.8 Proton spectra for various selected solar particle events (SPE) /Vahia and Biswas, 1983/.

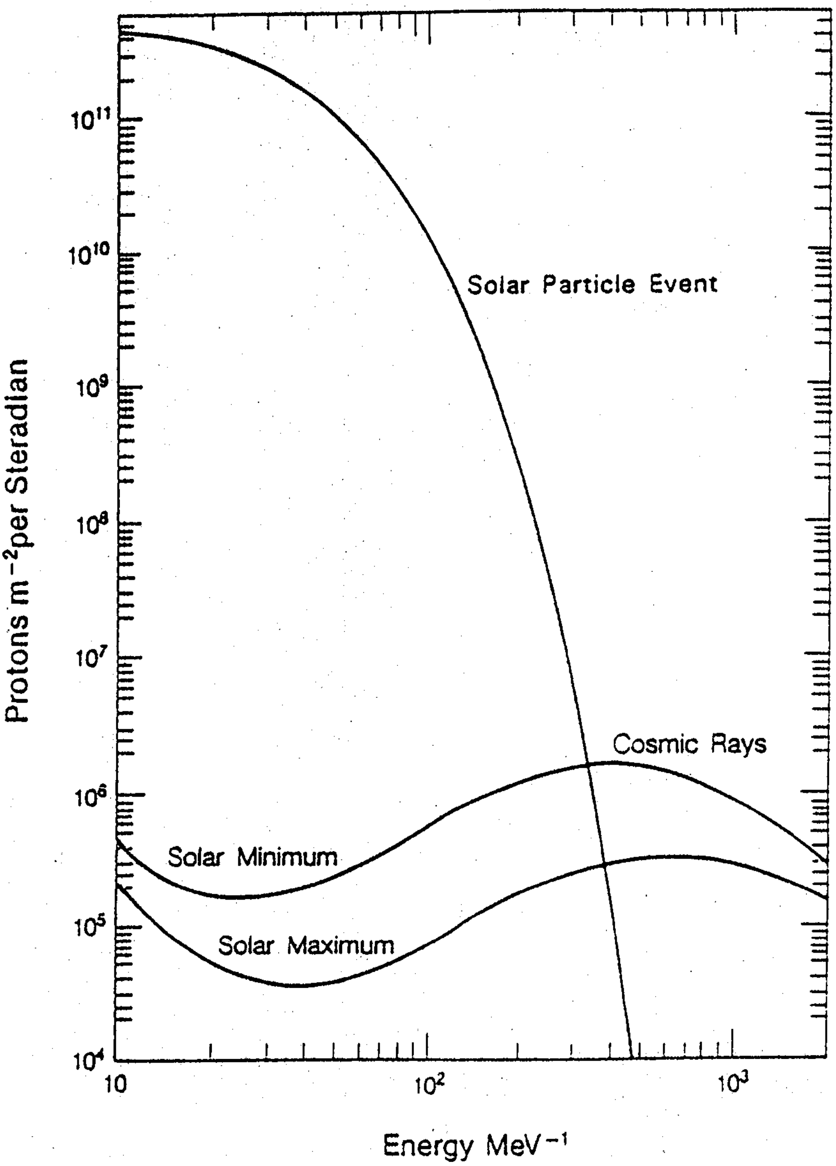

Fig. II.9 A comparison of the time-integrated differential energy spectrum of protons for the SPE of August 4 to 7, 1972 with the spectra of cosmic-ray protons accumulated in one week /Silberberg et al., 1984/.

III. PREDICTIONS OF LDEF FLUXES AND DOSE DUE TO GEOMAGNETICALLY TRAPPED PROTONS AND ELECTRONS

The current environment model in use is the "Vette" model /Sawyer and Vette, 1976; Teague and Vette, 1974; Teague *et al.*, 1976/ together with the associated magnetic field models /Stassinopoulos and Mead, 1972/. Given an orbital trajectory, the field models yield the magnetic field coordinates B and L. Given the B and L along the trajectory, the Vette model yields the omnidirectional flux along the trajectory as a function of energy. The proton environments used were AP8MIN and AP8MAX /Sawyer and Vette, 1976/, the electron environments were AE8MIN and AE8MAX /Teague and Vette, 1974; Teague *et al.*, 1976/ and the magnetic field model was the IGRF 1965.0 80-term /Stassinopoulos and Mead, 1972/ for solar minimum projected to 1964, the epoch of the environmental model, and the Hurwitz U.S. C&GS 168-term 1970 model for solar maximum at 1970. (The references provided for the electron environment document the previous models to AE8MIN and AE8MAX which had been undocumented). The Vette proton models have a large uncertainty (a factor of 2 in values of flux). The electron models have an even larger uncertainty (a factor of 6). To obtain the LDEF mission fluences shown in Table III.1 and Figs. III.1–III.4, we calculated long-term average fluxes for five circular orbits at 258.5, 255.0, 249.9 (at solar minimum), 230.0, and 172 nautical miles altitude (at solar maximum) which occurred on mission days 0, 550, 1450, 1950, and 2105 respectively and did a numerical integration over time assuming a straight line between time points.

The mission doses due to geomagnetically trapped particles are shown in Table III.2 and Figs. III.5 and III.6. The galactic cosmic ray dose contribution which is not included would add about 6 rad to these numbers. The mission proton doses were obtained from the mission fluences using the Burrell proton dose program /Burrell, 1964/ which is based on the "straight-ahead" and "continuous-slowing-down" approximations for transporting the protons. Two simple geometries were used–a point tissue receiver material at the center of a spherical aluminum shell and a point tissue receiver material behind a plane aluminum slab with infinite shielding behind the receiver. For the electron and bremsstrahlung dose we used the MSFC electron dose program /Watts and Burrell, 1971/ which is based on fits to data from the ETRAN electron Monte Carlo program /Berger and Seltzer, 1968/. It only performs the slab geometry. As an estimate for the spherical shell geometry we doubled the slab results which underestimates the actual result.

Tables III.1 and III.2, and Figs. III.1 through III.6 give the results of the calculations using the omnidirectional Vette models as described above. Figure III.7 uses, in addition, the directional model /Watts *et al.*, 1989/ as a "post-processor" of the Vette proton model to obtain an estimate of the magnitude of the proton anisotropy effect.

Table III.1 Geomagnetically Trapped Mission Fluences for LDEF

Energy (MeV)	Differential Proton Fluence (protons/cm^2-MeV)	Integral Proton Fluence (protons/cm^2)
0.05	$5.0\text{x}10^{8}$	$5.3\text{x}10^{9}$
0.25	$3.8\text{x}10^{8}$	$5.2\text{x}10^{9}$
0.50	$2.8\text{x}10^{8}$	$5.1\text{x}10^{9}$
1.0	$1.3\text{x}10^{8}$	$5.0\text{x}10^{9}$
1.5	$7.1\text{x}10^{7}$	$5.0\text{x}10^{9}$
2.0	$6.2\text{x}10^{7}$	$4.9\text{x}10^{9}$
2.5	$5.5\text{x}10^{7}$	$4.9\text{x}10^{9}$
3.0	$5.5\text{x}10^{7}$	$4.9\text{x}10^{9}$
3.75	$5.3\text{x}10^{7}$	$4.8\text{x}10^{9}$
4.5	$5.0\text{x}10^{7}$	$4.8\text{x}10^{9}$
6.0	$5.2\text{x}10^{7}$	$4.7\text{x}10^{9}$
10.	$4.6\text{x}10^{7}$	$4.5\text{x}10^{9}$
15.	$3.6\text{x}10^{7}$	$4.3\text{x}10^{9}$
30.	$3.0\text{x}10^{7}$	$3.8\text{x}10^{9}$
50.	$2.7\text{x}10^{7}$	$3.3\text{x}10^{9}$
100.	$2.0\text{x}10^{7}$	$2.1\text{x}10^{9}$
200.	$7.7\text{x}10^{6}$	$7.4\text{x}10^{8}$
300.	$2.7\text{x}10^{6}$	$2.6\text{x}10^{8}$
400.	$9.7\text{x}10^{5}$	$9.6\text{x}10^{7}$
600.	$1.3\text{x}10^{5}$	$1.3\text{x}10^{7}$

Energy (MeV)	Differential Electron Fluence (electrons/cm^2-MeV)	Integral Electron Fluence (electrons/cm^2)
0.05	$2.2\text{x}10^{13}$	$2.3\text{x}10^{12}$
0.25	$2.8\text{x}10^{12}$	$3.3\text{x}10^{11}$
0.50	$2.6\text{x}10^{11}$	$5.3\text{x}10^{10}$
1.0	$2.4\text{x}10^{10}$	$9.6\text{x}10^{9}$
1.5	$6.4\text{x}10^{9}$	$3.7\text{x}10^{9}$
2.0	$2.6\text{x}10^{9}$	$1.7\text{x}10^{9}$
2.5	$1.8\text{x}10^{9}$	$7.9\text{x}10^{8}$
3.0	$5.4\text{x}10^{8}$	$1.4\text{x}10^{8}$
3.75	$2.2\text{x}10^{7}$	$4.9\text{x}10^{6}$

Table III.2 LDEF Mission Dose due to Trapped Protons and Electrons Behind an Aluminum Shield for a Tissue Receiver

	Plane Slab–Infinite Backing			Center Spherical Shell		
Thickness (g/cm^2)	Electron (rads)	Proton (rads)	Total (rads)	Electron (rads)	Proton (rads)	Total (rads)
0.00	299000.0	4820.0	304000.0	598000.0	9641.0	608000.0
0.01	31900.0	668.0	32600.0	63800.0	1510.0	65300.0
0.02	15700.0	608.0	16300.0	31400.0	1390.0	32800.0
0.03	9510.0	572.0	10100.0	19000.0	1310.0	20300.0
0.04	6480.0	547.0	7030.0	13000.0	1270.0	14200.0
0.05	4600.0	526.0	5130.0	9200.0	1240.0	10400.0
0.06	3390.0	509.0	3900.0	6780.0	1210.0	7990.0
0.08	2030.0	481.0	2510.0	4060.0	1150.0	5210.0
0.10	1330.0	459.0	1790.0	2660.0	1110.0	3770.0
0.20	339.0	394.0	733.0	678.0	964.0	1640.0
0.30	140.0	358.0	498.0	280.0	882.0	1162.0
0.40	73.4	335.0	408.0	147.0	833.0	979.0
0.50	43.7	316.0	360.0	87.4	796.0	884.0
1.00	4.5	259.0	263.0	8.9	681.0	690.0
2.00	0.1	201.0	201.0	0.2	571.0	571.0
5.00	0.1	124.0	124.0	0.1	409.0	409.0
10.00		72.2	72.3	0.1	278.0	279.0
20.00		33.9	33.9		155.0	155.0
30.00		19.1	19.1		98.2	98.2
40.00		11.7	11.7		66.0	66.0

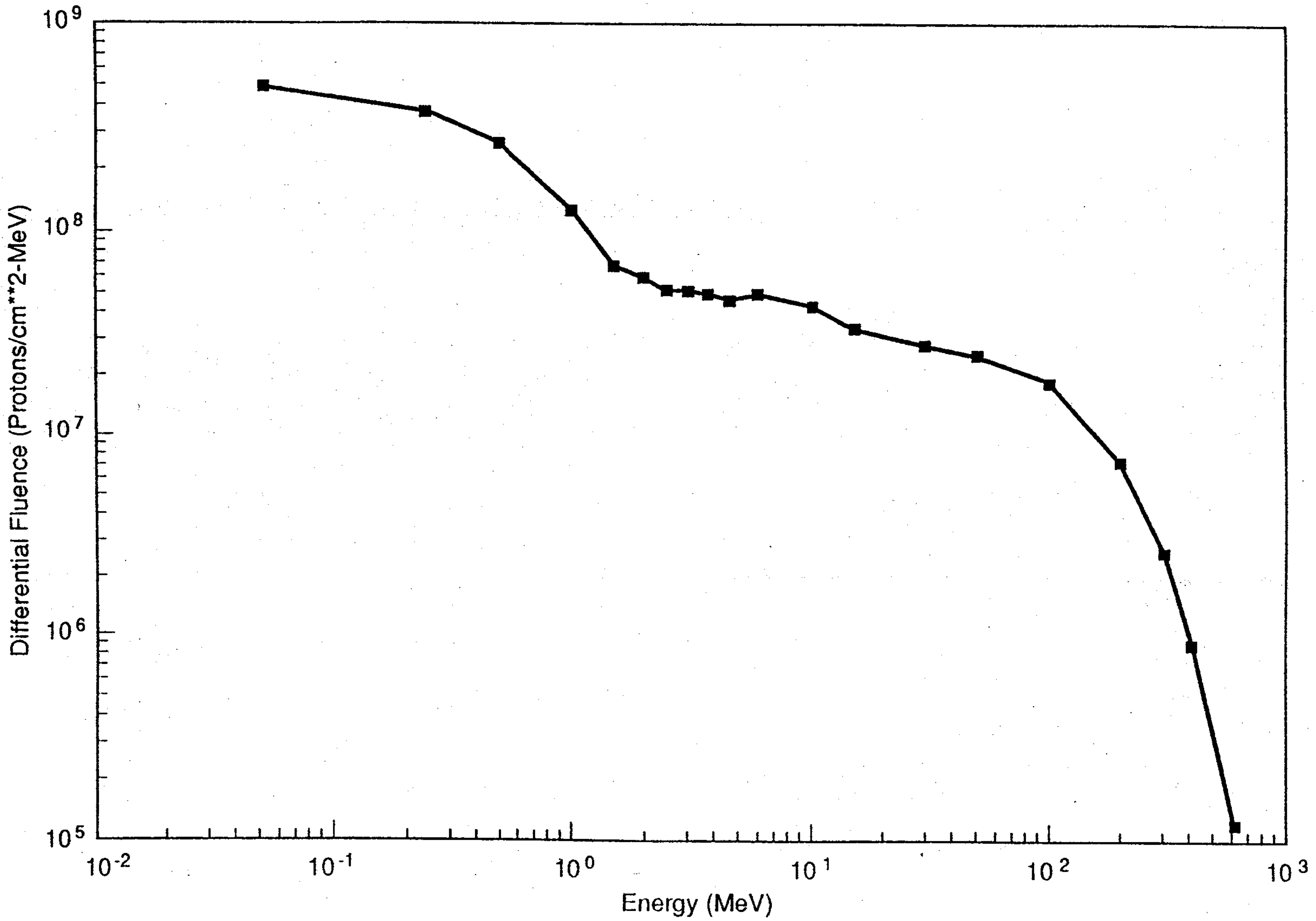

Trapped Proton Fluence for LDEF

Fig. III.1 The calculated LDEF mission trapped proton fluence in differential energy spectrum form. This spectrum was calculated using the LDEF altitude profile and proton models as described in Sections II and III.

5-11482-0-309

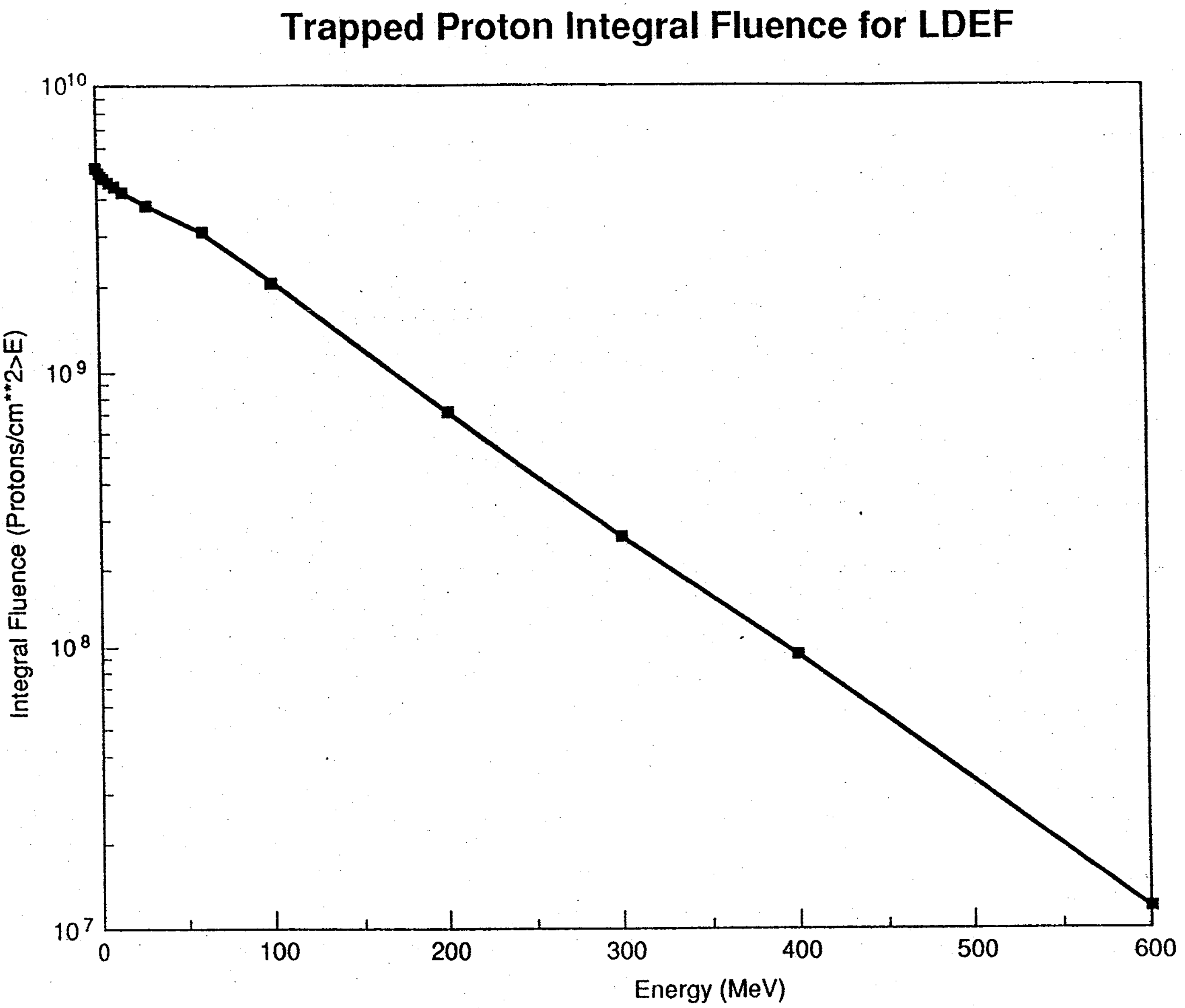

5-11487-0-309

Fig. III.2 The calculated LDEF mission trapped proton fluence in integral energy spectrum form. Methods of calculation are described in Sections II and III.

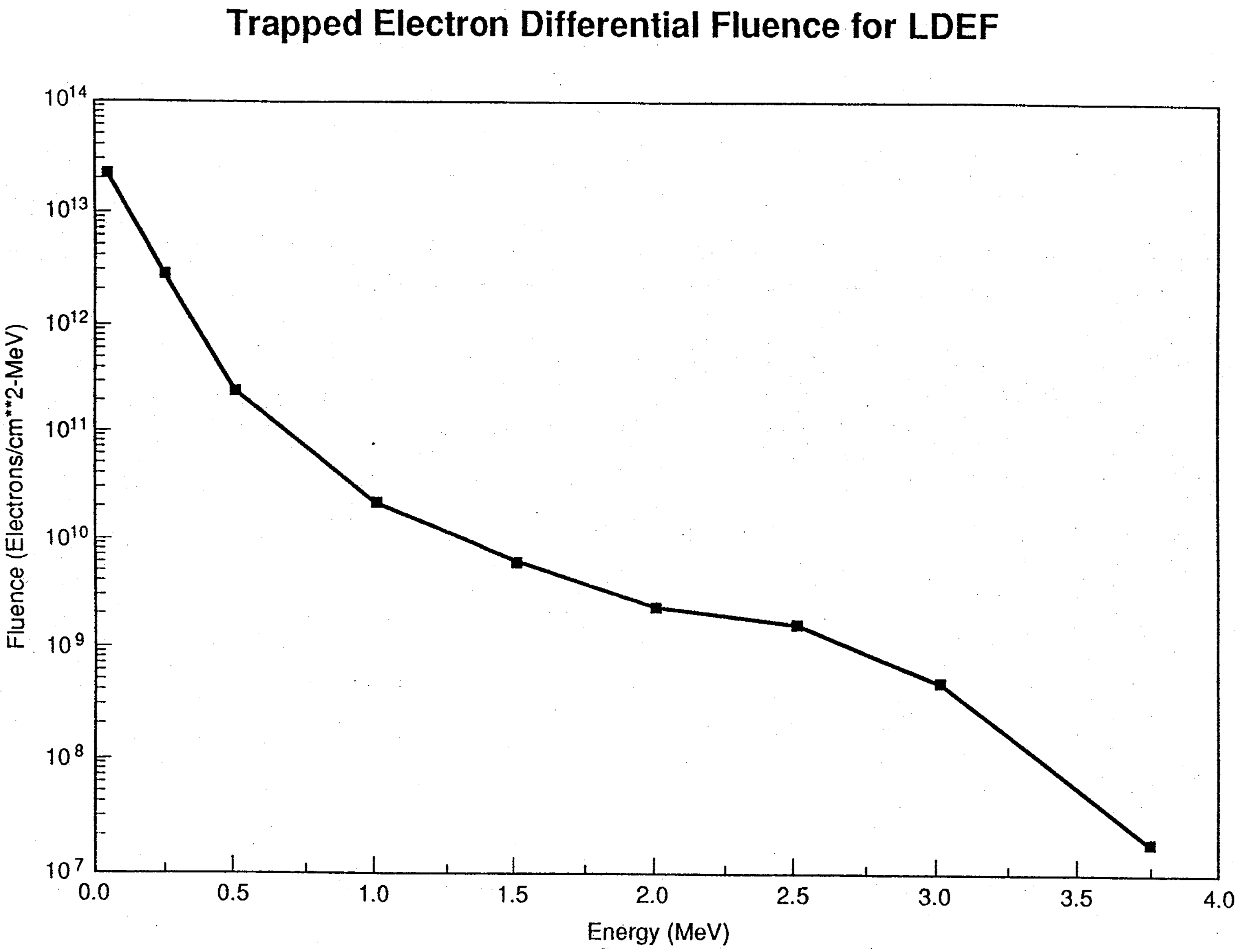

Fig. III.3 The calculated LDEF mission trapped electron fluence in differential energy spectrum form. The LDEF altitude profile was used and electron models as described in Sections II and III.

5-11485-0-309

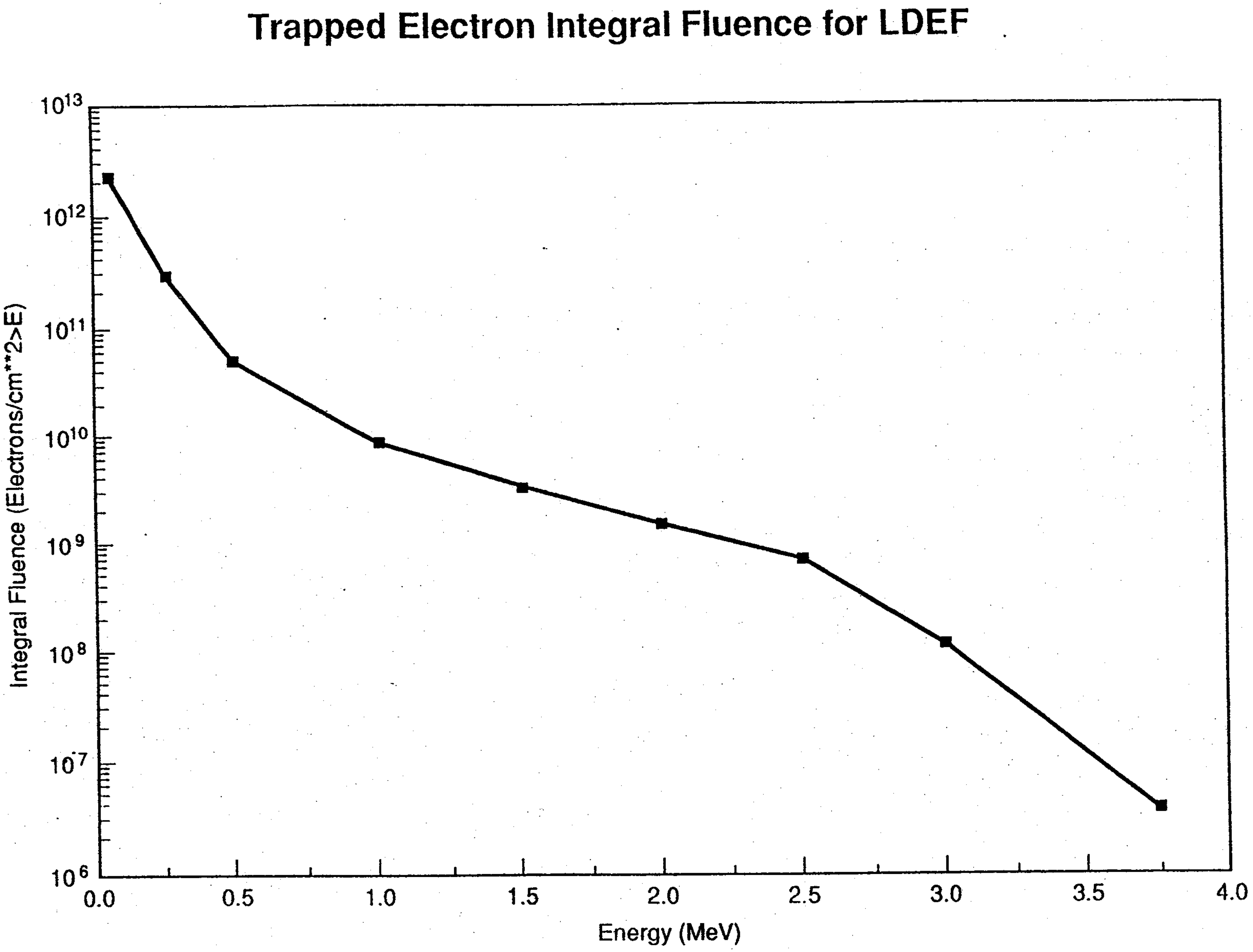

5-11486-0-309

Fig. III.4 The calculated LDEF mission trapped electron fluence in integral energy spectrum form. Methods of calculation are described in Sections II and III.

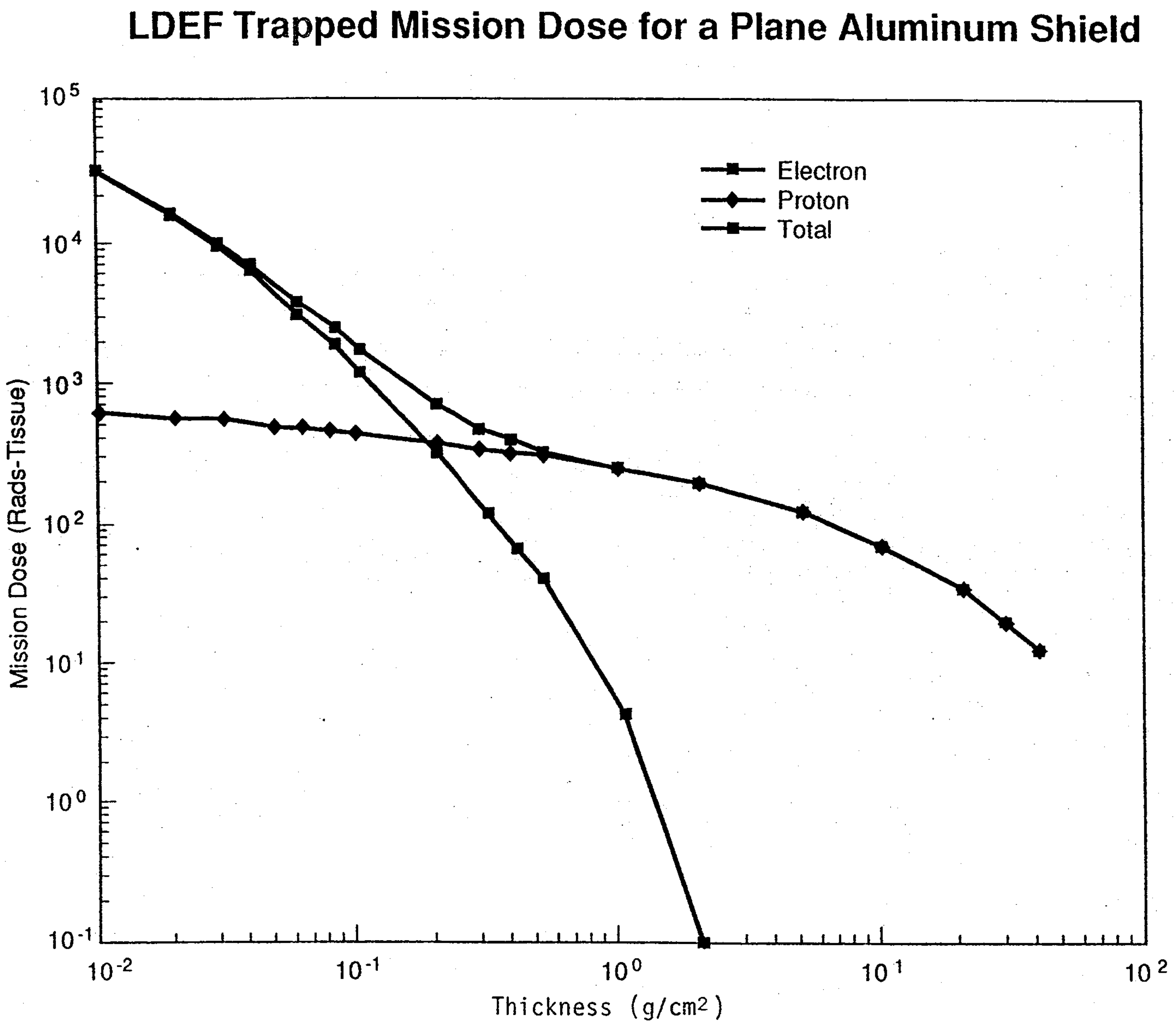

5-11484-0-309

Fig. III.5 The calculated LDEF mission absorbed dose from trapped protons and electrons, using the omnidirectional AP8 models with the temporal and altitude history of LDEF. The assumed shields were planes on one side of the dose point; the other side was shielded by an infinite shield. Methods are further described in Sections II and III. The calculated dose at the surface is ≈300 krad.

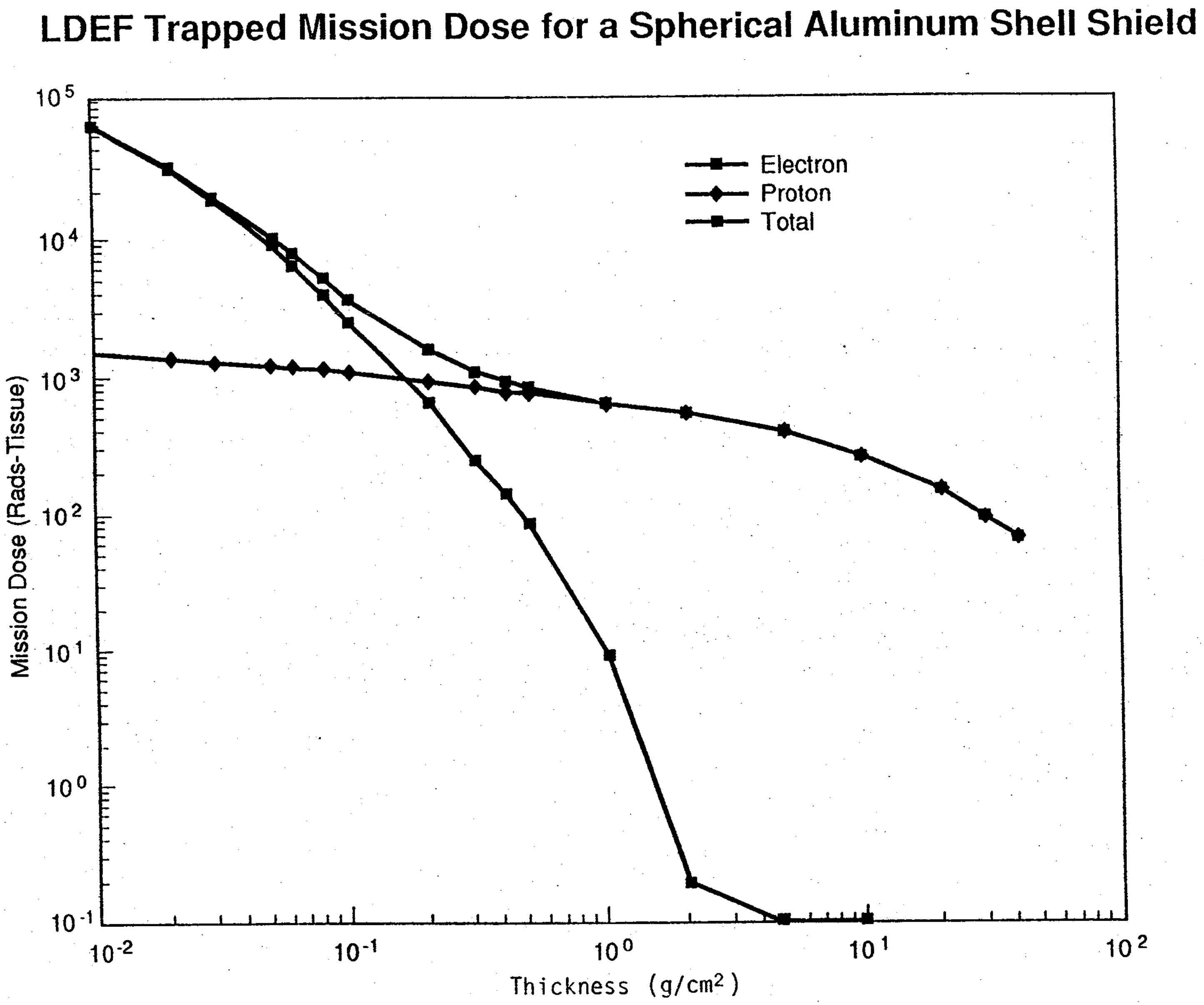

Fig. III.6 The calculated LDEF mission absorbed dose from trapped protons and electrons. The methods are the same as for Fig. III.5 except that spherical aluminum shells of various thicknesses (g/cm^2) were used as shields, with the dose values given at the center. The calculated dose at the surface is ≈600 krad.

5-11483-0-309

Calculated Radiation Dose Using Directional Model of Trapped Protons

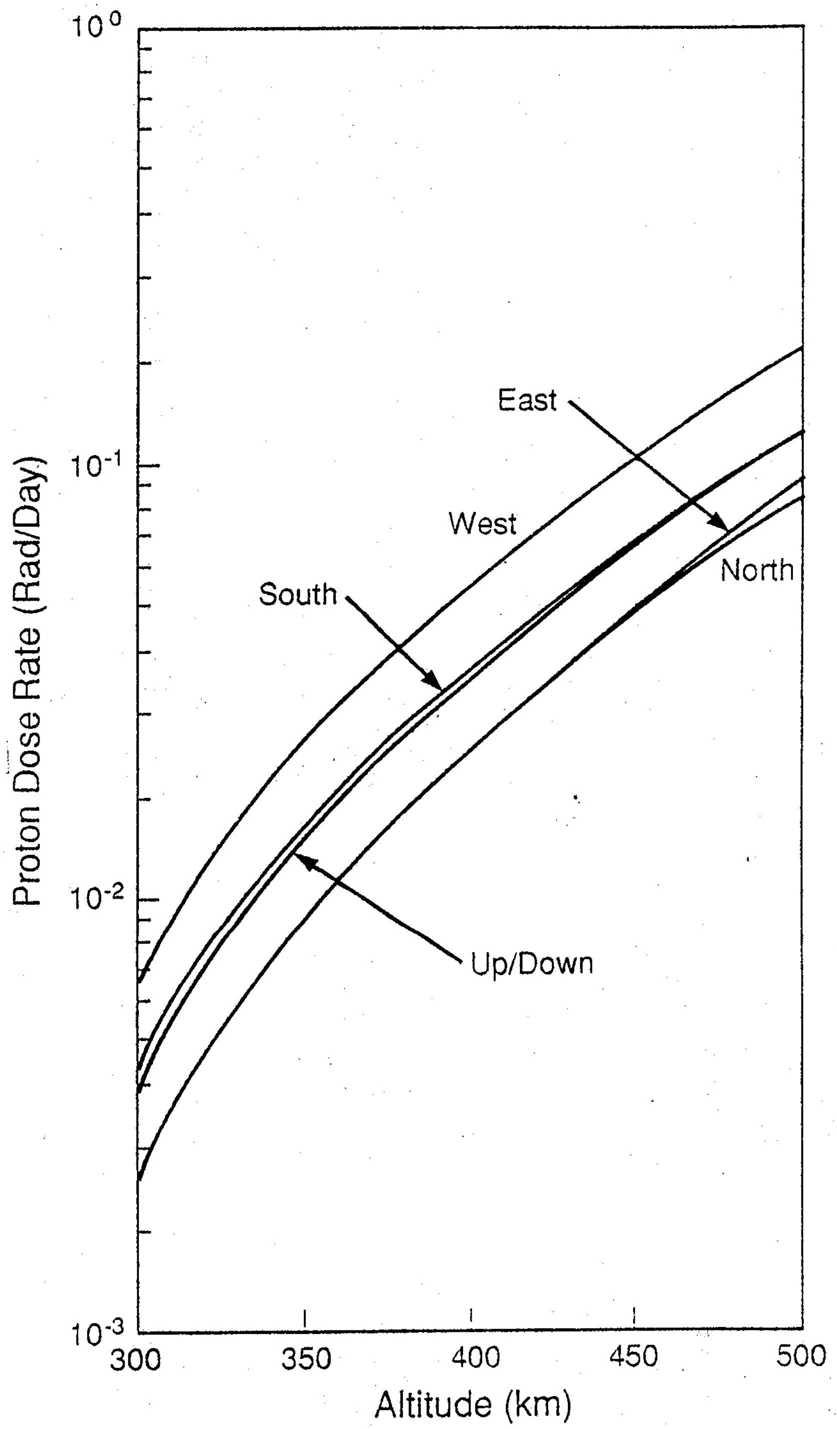

Fig. III.7 A calculation of trapped proton dose rate using the proton directional model of Watts et al. /1989/. The calculation uses the AP8 omnidirectional flux with a "post-processor" that converts to a vector flux and spectrum. The shield was 5 gm/cm^2 thick, with the normal pointed in the directions noted in the figure. The shield behind the dose point is infinite. Methods are discussed in Sections II and III and in Watts et al. /1989/.

IV. LINEAR ENERGY TRANSFER SPECTRA FOR THE LDEF MISSION

The "linear energy transfer" (LET) spectrum describes the variety of energy losses per unit path length that occur in a small volume of material exposed to a mixed radiation field. In the simplest case, the LET spectrum describes the relative frequency with which charged particles of various ionization energy losses (dE/dx) pass through the volume. The linear energy transfer has various definitions depending upon the application, and is described in some detail in Adams et al. /1986/ and in ICRU Report 16. LET spectra are applied in several contexts. In radiobiology, the spectra of LET are often used to describe the relative biological efficiency (RBE) of various mixed-field radiations to a given absorbed dose. LET dependent "quality factors" (QF) are often used to derive the radiation equivalent man-dose (rem) from LET spectra.

The LET spectra are also used to predict the temporal frequency of "single hit" phenomena. The frequency of hits by cosmic ray iron nuclei (high LET) in a chromosome may be related to observed genetic effects in some plants grown from space-exposed seed samples, for example. Heavily ionizing radiation can cause effects in electronic circuits by a transient production of free electrons in a microcircuit junction, or noise in a pixel of a charged-coupled imaging device. The frequency of "single event upsets" in microcircuits or noise in imaging devices can be determined from the LET spectra if the threshold LET (e.g., number of free electrons per unit path length) is known for the device in question.

We describe in this section the results of computations of the integral LET spectra at various shielding depths for the LDEF mission. The Naval Research Laboratory's Cosmic Ray Effects on Microelectronics (CREME) computer code /Adams et al., 1981, 1983a; Adams, 1986; Tsao et al., 1984/ was used to compute these spectra. (The galactic cosmic ray elements hydrogen through uranium are included in the CREME model). Trapped protons calculated using the AP8 environment model /Sawyer and Vette, 1976[1]/ were also included in some spectra. Also included in the CREME code is the singly-ionized anomalous component consisting of the elements helium, carbon, nitrogen, oxygen, neon, magnesium, silicon, argon and iron. The galactic cosmic ray component and the singly-ionized anomalous component are modulated by the solar wind in the interplanetary medium before their approach to the earth's magnetic field, and this is factored into the CREME code. The appropriate part of the solar cycle must be selected in CREME.

A significant part of the LDEF flight occurred during solar minimum. In the CREME code the solar activity is predicted by a sinusoidal fit to the ground level cosmic ray intensity at the Deep River neutron monitor located in Ontario, Canada. It is assumed that there are no magnetic disturbances (storms) on the sun for the LDEF calculations. At any rate, the

---

[1] The AP8 trapped proton data transmitted to me by J.W. Watts, Jr.

minimum energy of a fully stripped galactic cosmic ray for the LDEF orbit is a few GeV/amu, which excludes most of the solar particles. We have ignored the question of the existence of trapped heavy ions in the earth's radiation environment, "geomagnetically forbidden" cosmic ray particles, and any multiple-ionized cosmic rays in the anomalous component. The geomagnetic cutoff transmission function for the LDEF mission is approximated by applying the vertical cutoff to all cosmic rays regardless of their arrival direction. The vertical cutoff is roughly equal to the average value of the magnetic rigidity cutoff, averaged over all particle arrival directions for that particular position in the LDEF orbit. The geomagnetic cutoff transmission function is evaluated at 200 points along a circular orbit (481.5 km in altitude, 28.5° in inclination) and averaged over ~30 orbits. Since the LDEF was at a relatively low altitude, the earth's cosmic ray shadow was taken into account when computing the geomagnetic cutoff. Once the differential energy spectra of the galactic cosmic rays, trapped protons, and anomalous component have been defined at the surface of the LDEF, the only remaining task is to transport the combined charged particle spectrum through an aluminum equivalent shield to the detector material. At present the detector material in the CREME code is silicon, which represents microelectronic components. Any detector material may by modeled in the CREME program by constructing a particle stopping power vs. energy table for that material.

The transport method treats energy loss of the charged particles and particle losses due to nuclear collisions. However, collision fragments are not transported in this model; thus, this aspect of CREME gives a slight underestimate for an aluminum equivalent shielding between the values of 10 and 50 g/cm^2 and becomes progressively more serious above 50 g/cm^2 /Adams, 1983b/.

Fig. IV.1 shows the predicted orbit-average integral LET flux spectra at the spacecraft surface at LDEF insertion (481.5 km altitude, near solar minimum) and at LDEF recovery (370.4 km altitude, near solar maximum). As indicated, the major variation in the LET spectrum during the mission is from the trapped proton contribution.

Fig. IV.1 also shows that at the spacecraft surface the anomalous cosmic ray component makes a large contribution to the high-LET portion of the spectrum. Currently, there is considerable uncertainty in defining the anomalous cosmic ray environment, particularly with regard to the ion charge state. The calculations here assume the anomalous component to be singly ionized, which results in minimum geomagnetic shielding and maximum contribution to the LET spectrum.

Fig. IV.2 shows the depth dependence of the total LET spectrum including all components (trapped protons, galactic cosmic rays, and anomalous cosmic rays), and Fig. IV.3 shows the depth dependence of the galactic cosmic ray component only. Note from Fig. IV.2 that the anomalous component, which is comprised of relatively low energy ions, is attenuated rapidly with depth.

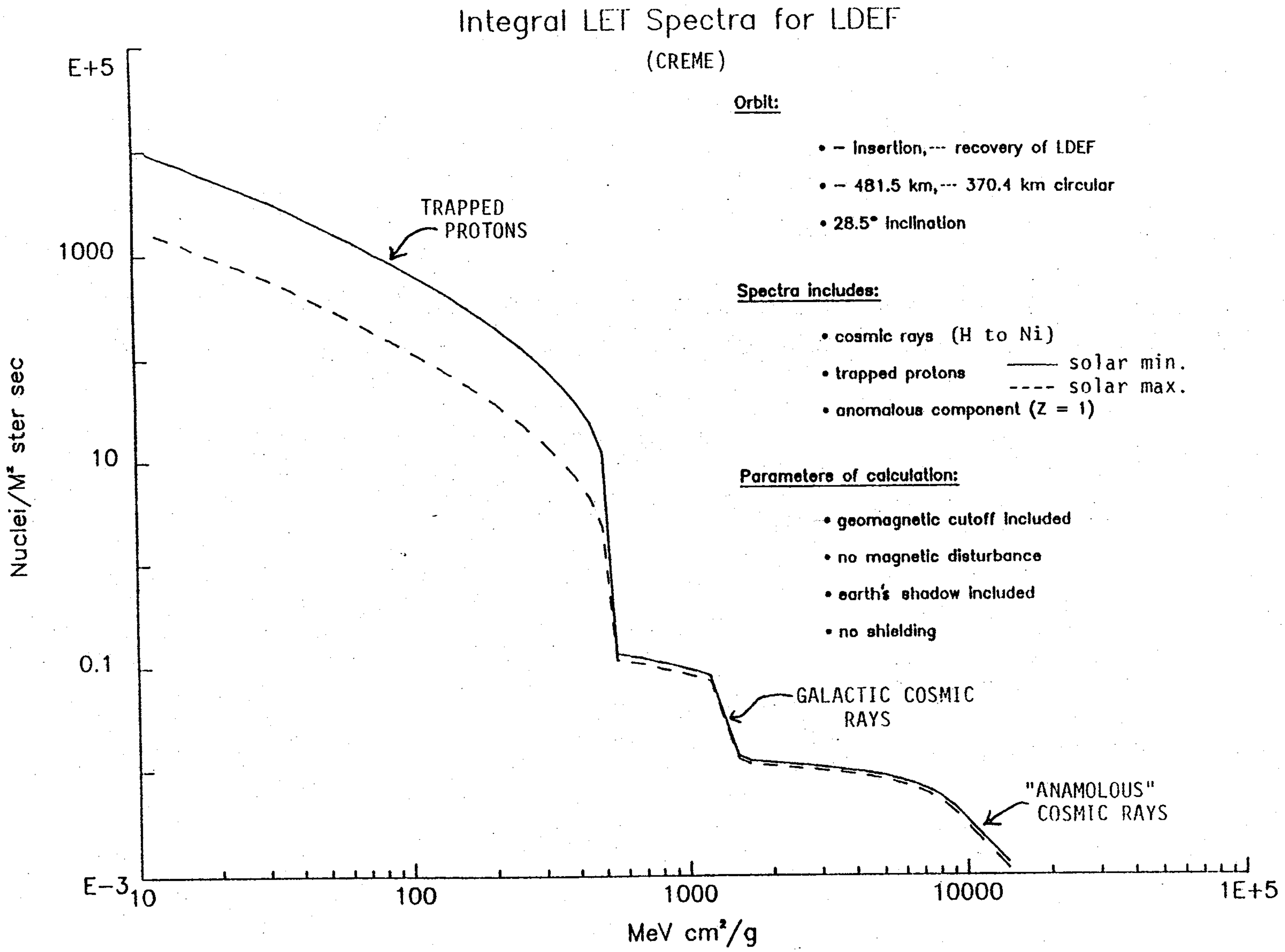

Fig. IV.1 The calculated total integral LET-spectra in silicon for the LDEF mission. The NRL CREME model (Sept. 1984 version) was used along with the AP-8 trapped proton environment (1970 epoch for solar maximum and 1964 epoch for solar minimum). The solar activity cycle was interpolated to reflect the actual launch and recovery dates.

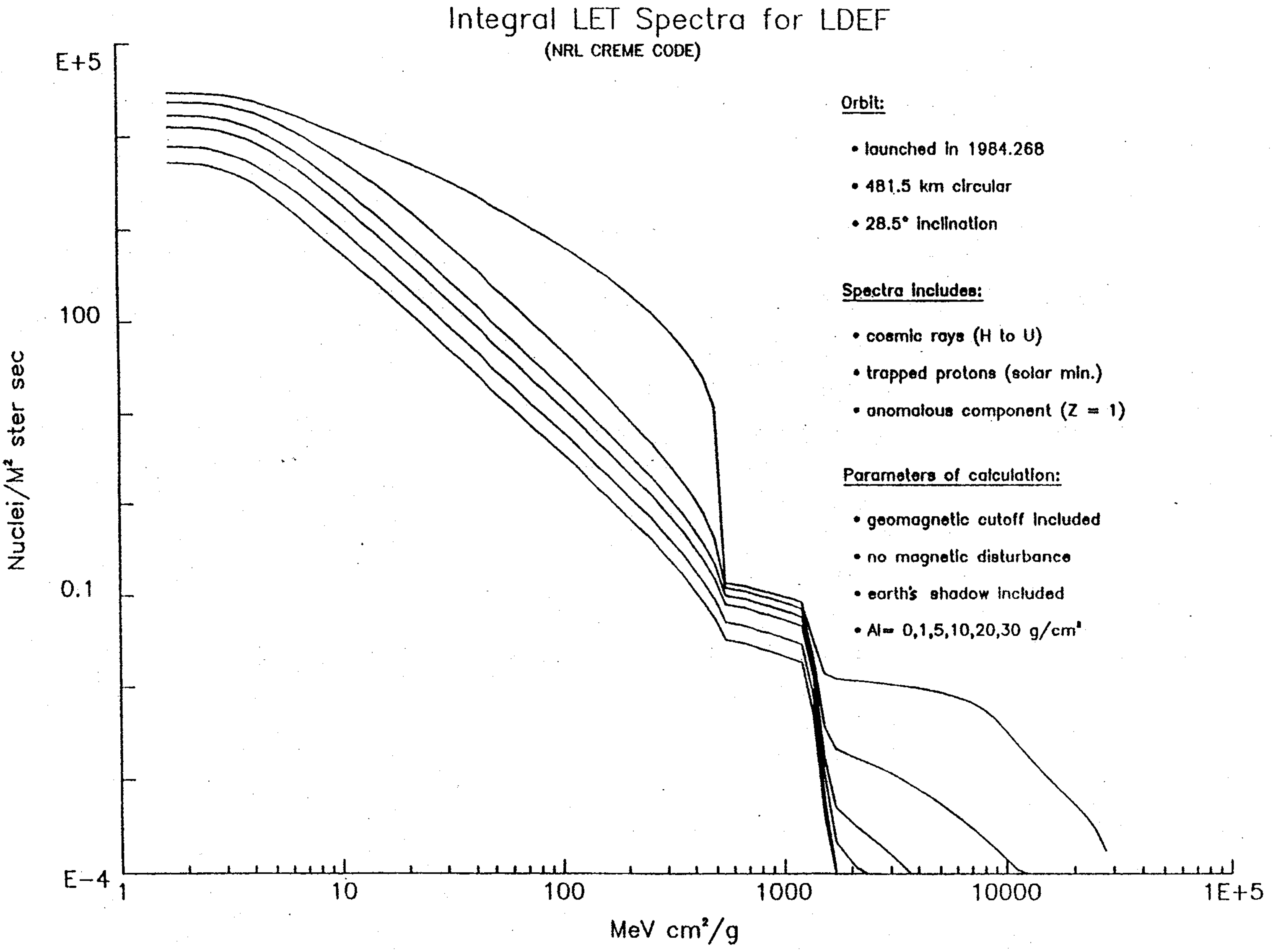

Fig. IV.2 The calculated total integral LET-spectra for the LDEF mission for a silicon detector at the center of an aluminum spherical shell whose thickness has been varied to encompass the detector shielding depths found in the various LDEF experiments. In this calculation, the solar activity was fixed at solar minimum.

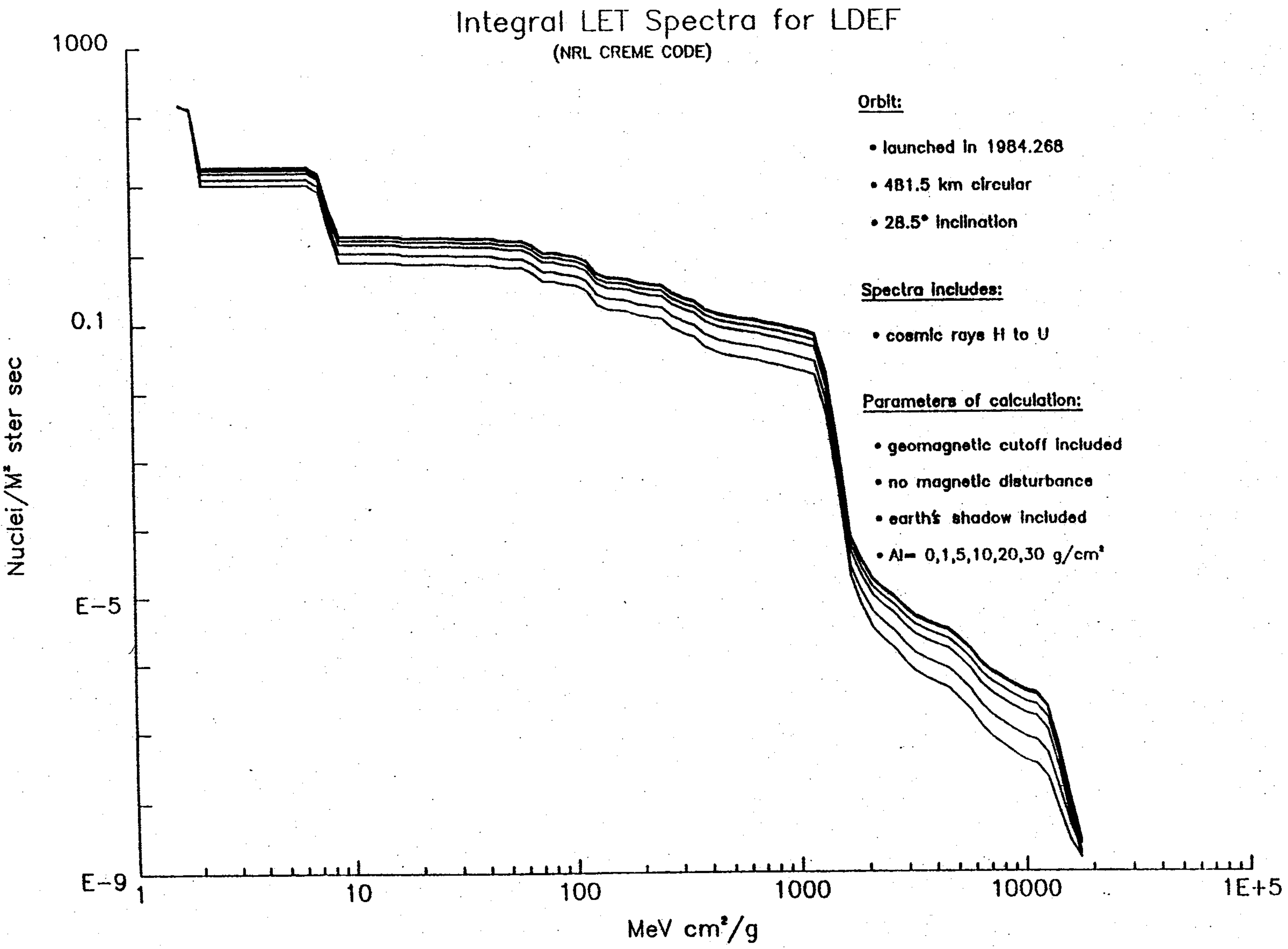

Fig. IV.3 The calculated galactic cosmic ray contribution to the integral LET-spectra for the LDEF mission which includes the elements hydrogen through uranium. Again, the solar activity is assumed to be at a minimum. The detector material was silicon.

V. NEUTRONS, SECONDARIES, SPALLATION PRODUCTS AND HIGH-LET RECOILS

Neutrons present in spacecraft are normally produced from interactions of GCR, and trapped protons with the spacecraft material, and there are also albedo neutrons coming from the atmosphere. The atmospheric albedo neutrons from cosmic ray interactions are the major source of inner belt protons, and their flux and spectrum have been calculated /Armstrong et al., 1973/ and also measured at energies above 2 MeV /Bhatt, 1976; Lockwood et al., 1976/. Predictions dealing with neutron levels inside spacecraft, taking the three sources into account as well as the transport through the shielding, are not currently available. However, a few spacecraft-based measurements have been made /Frank and Benton, 1987; Dudkin et al., 1990/.

Fast neutrons incident on tissue create a wide spectrum of LETs (see Fig. V.1) through the production of secondary protons, alpha particles and heavy recoiling nuclei, as well as gamma rays. Since the measurement of the charge and energy of short-range interaction products and recoil particles presently has limitations and uncertainties, evaluation of the dose due to those components depends more on calculations.

Calculations have been made of the absorbed dose and dose-equivalent for the secondary components from free space cosmic protons and for an SAA proton spectrum behind 20 g/cm^2 of aluminum /Armstrong et al., 1972; Santoro et al., 1972/. The dose contribution from secondary heavy nuclei, protons, pions, leptons and photons were individually calculated for depths up to 15 cm in tissue. In the case of the GCR protons, after ~2 cm depth, the dose-equivalents due to the secondary protons and secondary heavy nuclei both exceeded those due to the primary ionization of incident protons (~4 rem/yr from the secondary heavy nuclei). On the other hand, for the trapped protons, the secondary protons and heavy nuclei both contributed a dose equivalent of ~10% or more of the primary ionization. These results depended heavily 1) on the QFs used (a single Q = 20 for the heavy secondaries) and 2) on the intranuclear cascade model used to obtain the distribution of the heavy target fragments /Bertini, 1969/.

A calculation of the relative contribution of 592 MeV protons incident on a tissue-equivalent cylindrical phantom was performed by Armstrong and Bishop /1971/ and the results are shown in Fig. V.2. Here, the absorbed dose as a function of depth in tissue is shown for primary ionization, secondary protons, heavy nuclei, etc. Letaw calculated the dose and dose equivalent contribution for GCRs for the STS-51J (similar orbit to LDEF) mission as a function of aluminum shielding /Letaw et al., 1988/ (see Figs. V.3 and V.4).

Recently, experimental work using heavy energetic particle beams from accelerators has improved the knowledge of the distribution of the mass and energy of the heavy target fragments /Heckman, 1975; Greiner et al., 1975; Lindstrom et al., 1975/. The average fragment energy as a function of the fragment mass was reasonably well represented by calculational models /Bertini et al., 1972/. However, the fragment production cross-sections were different from those of the Bertini models, as shown in Table V.1. As a result, there is a large difference in the energy transfer cross sections (also displayed in the table). Greater differences will appear in the dose-equivalent because of the high QFs at high LET values as shown in Fig. V.5 /Wilson et al., 1989/. The energy transfer cross sections in Fig. V.5 are for single nuclear collisions of 2 GeV protons in water. Contributions from alpha particles derived from the Bertini model are included. Although the total event energy deposited differs by a factor of ~35%, the highest LET components differ by a factor of three.

Since some effects such as SEUs in computers and some biological effects are fluence-dependent, the assessment of risk from these components needs further work in measurement, calculations, and radiobiological studies. Some aspects of the secondary particles will be measured directly by LDEF experiments. The measurement of the neutron fluence and spectrum is an objective in several experiments (see Section I). Charged particle LET spectra, measured to unprecedented statistical accuracy on LDEF, should exhibit features that are due to secondaries. These will serve as data bases against which specific calculations of secondaries may be tested. The "High Energy Transport Code" (HETC), which will be used to calculate the induced radioactivity, is one of the predictive methods to be tested.

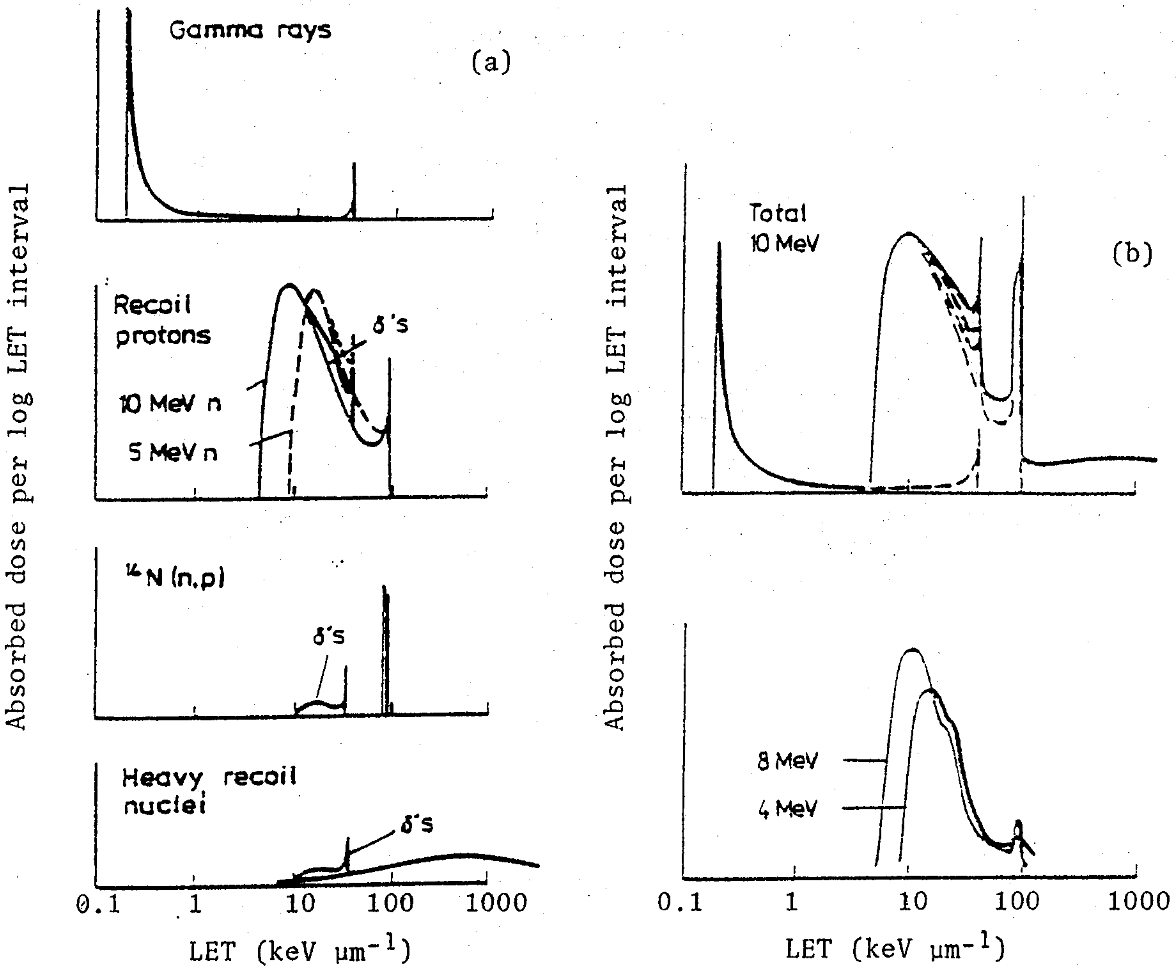

Fig. V.1 (a) Calculated distributions of absorbed dose vs LET for the four processes of energy absorption in tissue from fast neutrons. (b) Upper: summed distribution of dose vs LET for 10 MeV neutrons. Lower: measured distributions of dose in a low-pressure gas proportional counter simulating a sphere of unit-density tissue of 0.75 μm diameter /Fowler, 1981/.

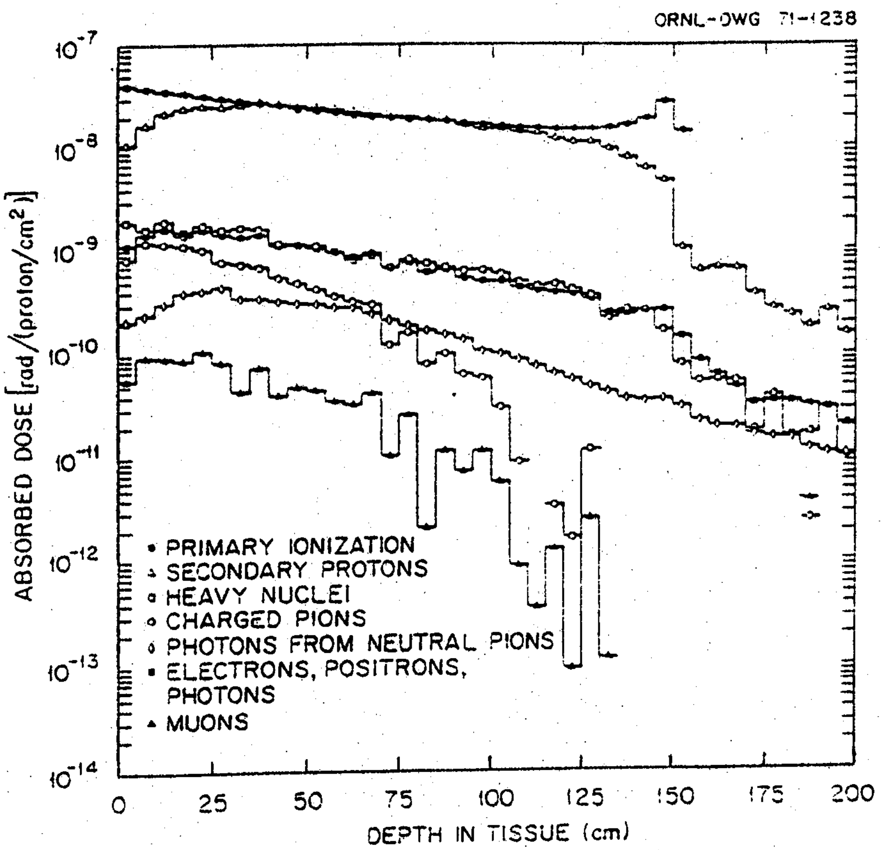

Fig. V.2 Contribution of various particles to the absorbed dose for 592-MeV protons incident on a cylindrical phantom /Armstrong and Bishop, 1971/.

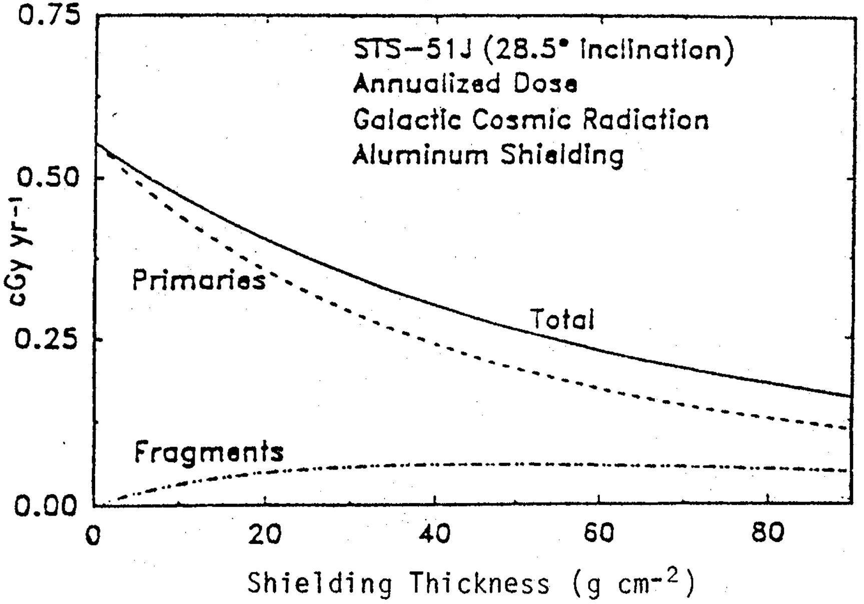

Fig. V.3

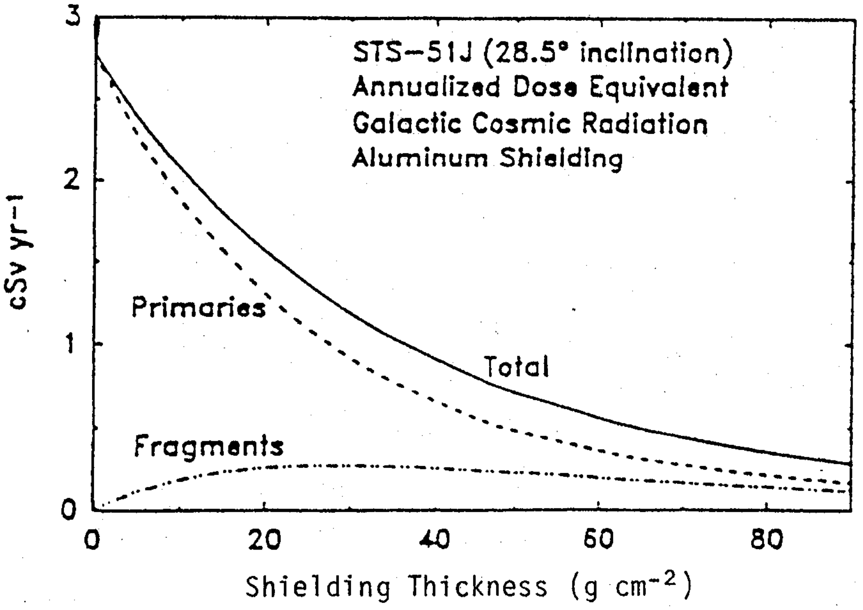

Fig. V.4

Figs. V.3, V.4 Annualized absorbed dose and dose equivalent for STS-51J. /Letaw, 1988./

Table V.1* Comparison of fragmentation cross sections (mb) and fragment energy transfer cross sections (MeV-mb) of Bertini with experiments /Greiner et al., 1975/.

A_F	$\sigma_{BERTINI}$	$\sigma_{GREINER}$	$\bar{E}\sigma_{BERTINI}$	$\bar{E}\sigma_{GREINER}$
16	4.69	.02	5.04	.0006
15	103.4	61.5	60.6	56.9
14	40.0	35.4	48.8	51.7
13	18.5	22.8	37.6	48.3
12	32.2	34.1	85.8	68.2
11	8.2	26.4	37.9	99.1
10	11.0	12.7	52.8	62.0
9	1.2	5.2	6.5	25.7
8	.56	1.23	2.5	7.1
7	1.06	27.9	6.11	153.4
6	5.46	13.9	31.4	73.4
Total:	226.3	241.2	375.1	645.8

* Average integral energy transfer cross sections as a function of the LETs of heavy target products for a 2 GeV proton incident on water / Wilson and Townsend, 1989/.

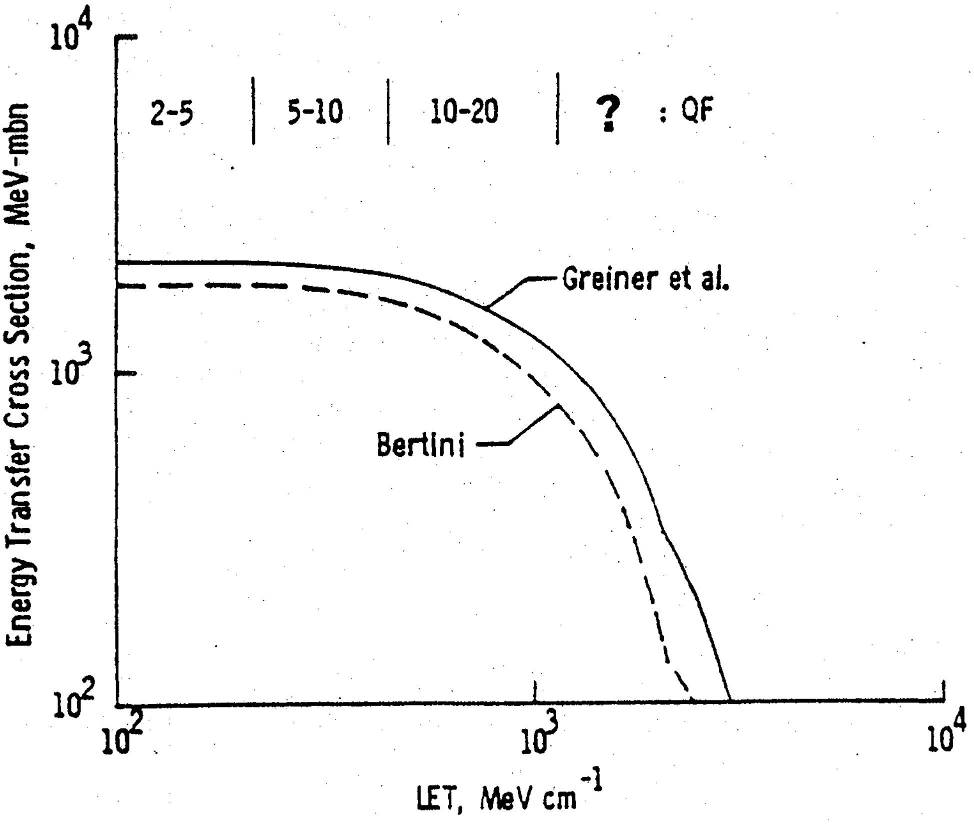

Fig. V.5 Calculations from the Bertini model and derived from Greiner et al., 1975, are shown along with approximate quality factors for various LET regions /Wilson et al., 1989/.

VI. INDUCED RADIOACTIVITY IN LDEF

Many materials become slightly radioactive when irradiated by the high energy protons of the trapped radiation belt and the cosmic ray protons and nuclei. These primary particles also produce secondary neutrons that activate some materials. The activation product of most interest is gamma radiation from radionuclides with half-lives of a few hours to a few years. With sufficiently long space exposures, these build up to "saturated activities" at which level the production is equalled by decay. Beta decay may be an associated process but the short range electrons usually stop in the material that contains the radionuclides, whereas the gamma rays have sufficient range that they may be detected within and outside the spacecraft.

The induced radioactivity produces a negligible radiation dose compared to the primary particles. Measurements on spacecraft, lunar, and meteoritic materials after return to earth have shown that materials exposed in low earth orbit and outside the earth's magnetosphere have very small specific activities ($\sim 10^{-10}$ to $\sim 10^{-8}$ curie/kg) and pose no health hazard.

Nevertheless, the activity does present a large and time-varying background to gamma ray astronomy experiments, which has motivated numerous studies of this phenomenon. The activation process also offers a passive method of determining the activating proton and neutron fluence that is immune to temperature effects and some problems of other passive techniques. Secondary neutrons are notoriously difficult to measure accurately in the presence of the primary protons and nuclei that produce them, and the measurement of activation offers some unique signatures of neutron fluence.

Studies of activation have been carried out in the past for meteoritic materials, planetary surfaces, material samples carried into space for such study, and spacecraft material of opportunity upon return or reentry. Some of the past studies include Dyer *et al.* /1988/, Fishman and Meegan /1980/, Fishman *et al.* /1989/, Michel and Stuck /1984/ and Reedy and Arnold /1972/.

LDEF offers significant and unique opportunities for the study of activation and associated nuclear processes in spacecraft material. These result from the long life in orbit, the stability with respect to earth and flight vector, the variety and spatial distribution of materials on board, and the return of the entire spacecraft. The long life allows the study of some long-lived nuclides which will build up to higher activity than previously available. For example, the study of ^{60}Co (5.26 years) in cobalt samples will allow the secondary neutron fluence in a large spacecraft to be determined with unprecedented sensitivity. The stability with respect to earth and the flight vector (similiar to Space Station) will allow the effects of the highly directional trapped proton flux to be studied. The many materials on board at different depths and locations will allow the activation due to protons and neutrons to be separated, and the secondary neutron fluence in a spacecraft to be determined more accurately than in previous measurements.

The radioactivity measurement and analysis plan for LDEF includes calculations to match the data, and also to determine the activating fluences for later use in extrapolating the LDEF experience to other orbits and situations. Calculations of activation involve the nuclear interaction process which also produces short range target spallation products of high specific ionization. These short range particles are difficult or impossible to measure, and calculations of their spectra will be valuable for studies of electronic circuit "single event upsets" and biological "single hit" phenomena.

The LDEF activation measurements and analysis program will provide a wealth of information for those planning future gamma ray or neutron experiments on spacecraft, for assessment of the effects of trapped proton directionality, and for studies of single hit phenomena in circuits, sensors, and biological systems.

The LDEF induced radioactivity measurement plan includes the following elements:

A. Individual sample measurements with high resolution gamma ray spectrometers in low background facilities. Several hundred samples weighing ~100 grams will be measured with detectors in eight laboratories.

B. Full spacecraft measurements in the recovery facility (SAEF II at KSC) before disassembly, with sensitive high resolution gamma ray detectors.

C. Calculations of induced activity of the major materials of interest using predicted trapped proton and cosmic ray fluences and spectra.

D. Assembly of a mass model and a radioactivity model of LDEF.

E. Calculation of gamma flux and spectrum and radiation dose to be expected in measurement *B*. Extrapolation to hypothetical exposure in high altitude orbits. Also calculation of the activity of short half-life nuclides and estimation of radiation dose due to activation gamma rays in orbit.

In the absence of detailed calculations of activation in LDEF, the best estimates are derived from measurements on material that has been exposed in low earth orbit. Skylab IV carried activation materials for a two month exposure /Fishman, 1976/, and a detailed analysis was made. Skylab debris recovered in Australia was also measured /Fishman and Meegan, 1980/. From these measurements, and extrapolation to the LDEF situation, it is predicted that LDEF will have gamma emitting activity in various materials ranging from 1 to 10 decays/kg-sec. The most prominent nuclide will be ^{22}Na, a spallation product of aluminum. The entire LDEF will have an activity of ~1 to 5 μcuries. This activity, spread throughout the large structure, will be detectable with only the most sensitive high resolution gamma ray detectors, and will not exceed the general gamma ray background in the recovery facility.

VII. LDEF RADIATION EXPOSURE AS PROJECTED FROM SHUTTLE MISSIONS

Independent of the calculational estimates discussed in previous sections, a general indication of the LDEF radiation exposure can be obtained by scaling the results of measurements made on Shuttle flights flown at the same 28.5° inclination as LDEF. Measurements from passive detectors flown on two 28.5° inclination Shuttle missions are discussed here: Shuttle mission STS-41C (in 1984, the mission that launched LDEF) and Shuttle mission STS-51J (in 1985), which had about the same altitude (510 km) as the initial LDEF orbit. It should be emphasized that these Shuttle results provide only rough estimates of the LDEF exposure because the shielding for the Shuttle dosimeters is generally larger than for the LDEF dosimetry locations.

VII.1 Projected Shuttle Dose and Fluence Measurements

Tables VII.1 and VII.2 list the total dose (from TLD measurements), HZE particle fluences and dose, and low-energy neutron dose equivalent measured on missions 41C and 51J, respectively. The numbers represent a simple scaling from the Shuttle mission length to the LDEF mission length of 2115 days. The "maximum on-board" doses were measured by the Passive Radiation Detectors (PRDs) at a location denoted as DLOC 2, which is located on the outside wall of the mid-deck compartment and has the least shielding of all of the six PRD locations. The LDEF exposures are expected to be generally higher since the Shuttle contains considerably more shielding.

VII.2 LET spectra

VII.2.1 Measurements

LET spectra in the range of ~5–1000 keV/μm (H_2O) have been measured on a variety of STS missions using CR-39 track detectors. LET spectra for 28.5° inclination orbits were measured for the STS-51J and the STS-61C flights by the University of San Francisco (USF) group using stacks of plastic nuclear track detectors (Figs. VII.1 and VII.2). Galactic cosmic ray nuclei (GCR, curve "B") can be identified in these experiments due to their high energies, which result in long-range trajectories through the stack and coincidences of etch cones over a large number of detector foils. Other events depositing high LET can be distinguished from the GCR by their short-range trajectories (SR, curve "C"), which have etch cone coincidences on the surface of only two adjacent detectors.

The STS-61C is a typical low altitude (324 km), 28.5° inclination orbit mission where a larger fraction of the exposure is from GCRs, as opposed to the STS-51J mission which is similar to the LDEF orbit. As can be seen in Fig. VII.1, the STS-51J fluxes are primarily the result of exposure to trapped protons and are manifested by high densities of short-range tracks in plastic track detectors (Curve C, Fig. VII.1). Again, the substantial difference in shielding between the orbiter (Atlantis) and the LDEF spacecraft needs to be kept in mind.

VII.2.2 Calculations

A set of programs that was developed more than ten years ago at Siegen allows the calculation of LET-spectra of cosmic ray nuclei /Heinrich, 1977/. These programs, in the following called the "Siegen LET Code," consider the effects of solar modulation, geomagnetic shielding, earth shadowing, and material shielding. Details of the procedures used in these types of calculations are described in a review article by W. Heinrich /1988/.

The Siegen LET code uses the models of Adams *et al.* /1981/ to describe the cosmic ray environment and solar modulation. The shielding effect of the earth's magnetic field is determined from a geomagnetic cutoff probability /Heinrich and Spill, 1979/ which involves using the worldwide cutoff rigidities calculated by Shea and Smart /1975/. Material shielding takes into account the effects of energy loss and nuclear fragmentation by using a system of propagation equations /Allkofer and Heinrich, 1974/. Fragmentation cross sections needed for these calculations are based on the empirical cross section formula of Silberberg and Tsao /1973/ for a hydrogen target, with scaling for heavier targets based on the factorization law discovered by Lindstrom *et al.* /1975/. Comparisons of the Siegen code with LET spectra calculated by the CREME code (described in Sec. IV) generally show good agreement.

VII.2.3 Comparisons of calculated and measured LET spectra for Shuttle flights

Cosmic-ray LET spectra calculated using the Siegen LET code are shown in Figs. VII.3 and VII.4 for Shuttle missions STS-51J and STS-61C, respectively. Comparing these calculated spectra with the measured galactic cosmic ray contribution (spectra "B") of Figs. VII.1 and VII.2, we find agreement for a calculated average shielding thickness of about 60 g/cm^2 aluminum equivalent for mission STS-51J and agreement at about 50 g/cm^2 for mission STS-61C. These numbers are higher than typical spacecraft shielding (10–20 g/cm^2) but not unrealistic. The difference between the predictions and measurements probably reflects the uncertainties in the incident cosmic ray flux spectra. Nevertheless, the general agreement justifies the basic calculational procedure and the measurement technique of using etch cone coincidence to separate out the GCR component of the LET spectrum.

TABLE VII.1

LDEF: PROJECTED RADIATION QUANTITIES FROM STS-41C

LDEF:	Launch Date:	6 April 1984
	Re-entry Date:	20 January 1990
	Altitude:	479-324 km
	Inclination:	28.5°
	Duration:	2115 days (5.790 yr)

Projected from STS-41C (alt. 528 (max)km, incl. 28.5°, dur. 168 hr)

A. Total Doses (TLDs)

APD	130 rad
Crew (min)	130 rad
Crew (max)	180 rad
Max On-Board	290 rad

B. HZE Particles*

Total Track Fluence (CR-39)	4.3×10^4 cm^{-2}
GCR Track Fluence	2700 cm^{-2}
S-R Track Fluence	4×10^4 cm^{-2}
Dose Equivalent	22 rem (220 mSv)
Dose	2.4 rad (24 mGy)

*$LET_\infty \cdot H_2O \geq 5$ keV/μm

C. Neutrons (Thermal and Resonance)

Dose Equivalent	1 rem (10 mSv)

TABLE VII.2

LDEF: PROJECTED RADIATION QUANTITIES FROM STS-51J

LDEF:	Launch Date:	6 April 1984
	Re-entry Date:	20 January 1990
	Altitude:	479-324 km
	Inclination:	28.5°
	Duration:	2115 days (5.790 yr)

Projected from STS-51J (alt. 510 (max)km, incl. 28.5°, dur. 95 hr)

A. Total Doses (TLDs)

APD	150 rad (est.)
Crew (min)	170 rad
Crew (max)	270 rad
Max On-Board	400 rad

B. HZE Particles*

Total Track Fluence (CR-39)	2.5×10^5 cm^{-2}
GCR Track Fluence	8.5×10^3 cm^{-2}
S-R Track Fluence	2.4×10^5 cm^{-2}
Dose Equivalent	36 rem (360 mSv)
Dose	5.5 rad (55 mGy)

*$LET_\infty \cdot H_2O \geq 5$ keV/μm

C. Neutrons (Thermal and Resonance)

Dose Equivalent	2 rem (20 mSv) (est.)

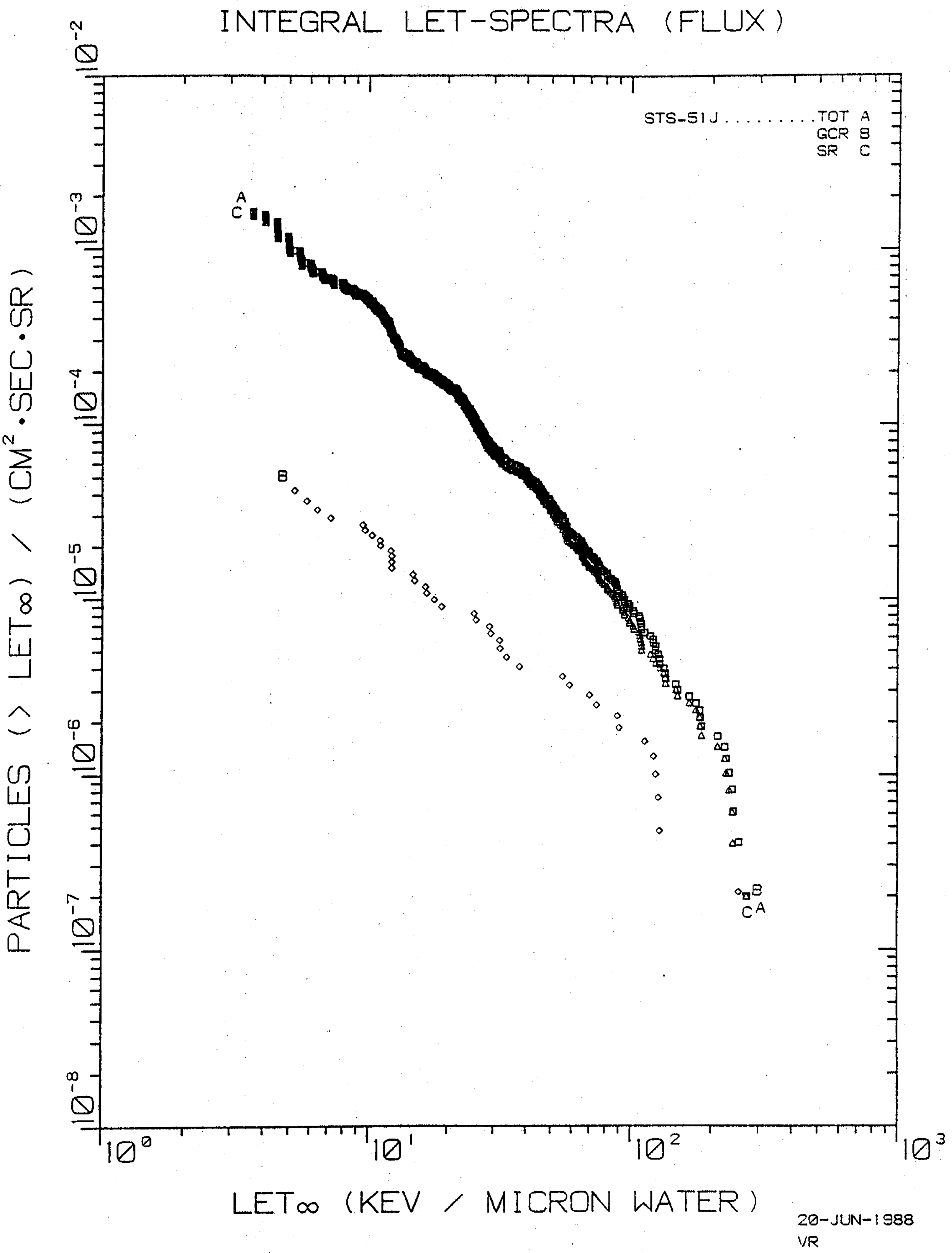

Fig. VII.1 Integral LET flux spectra for Total, GCR and SR particles measured on STS-51J. Note: the exposure is completely dominated by short-range (SR) events.

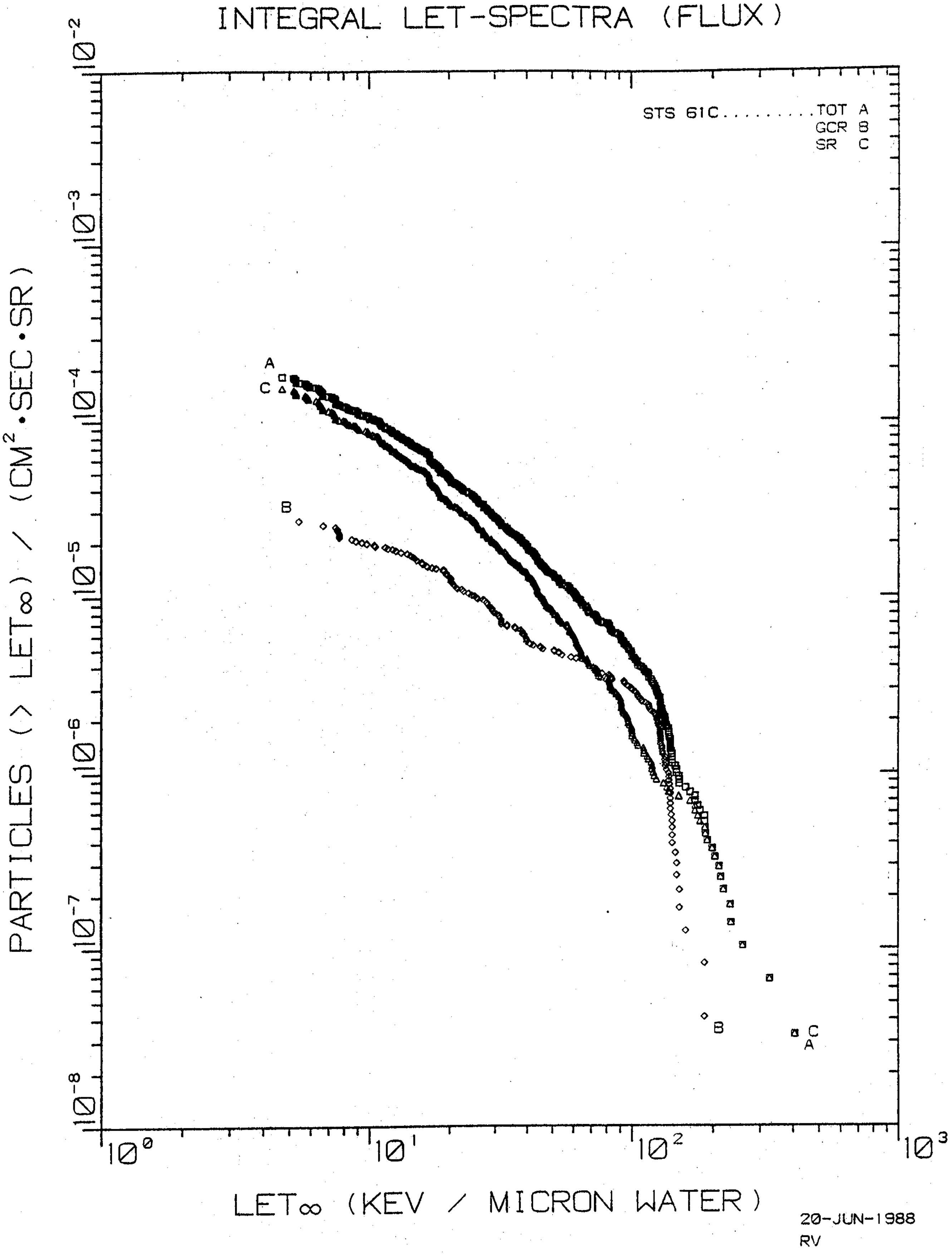

Fig. VII.2 Integral LET flux spectra for Total, GCR and SR particles measured on STS-61C.

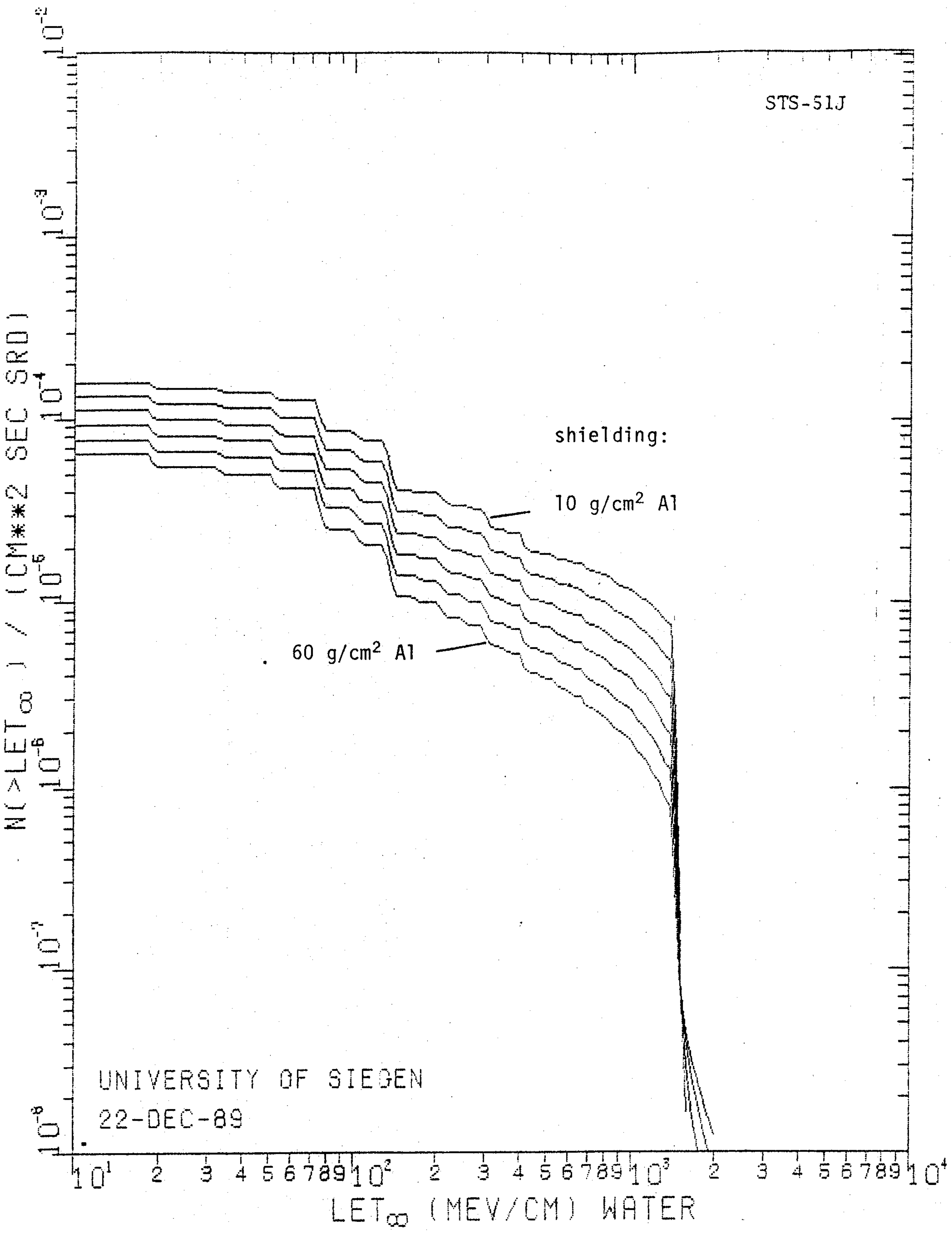

Fig. VII.3 Calculated LET spectra of galactic cosmic rays for mission STS-51J.

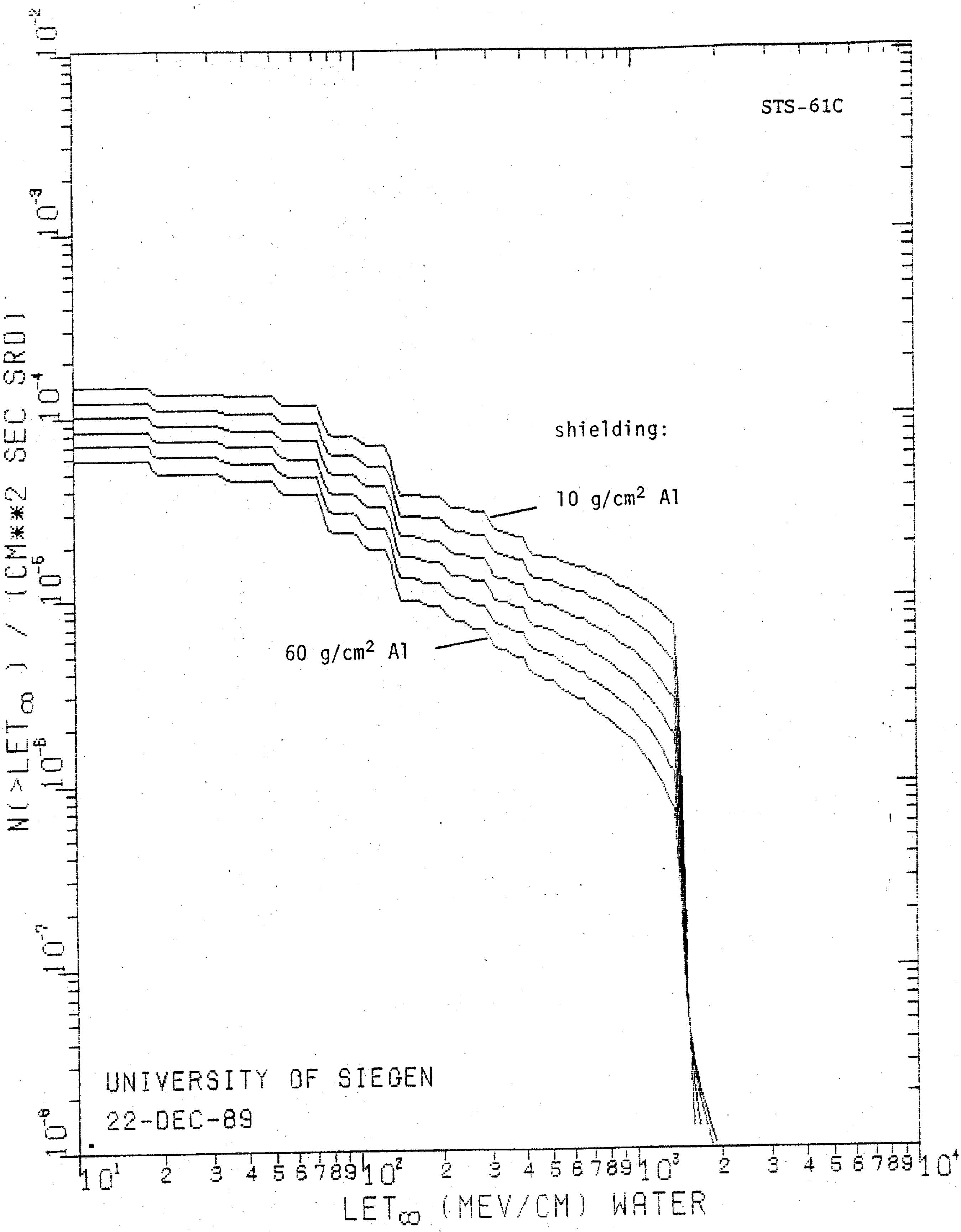

Fig. VII.4 Calculated LET spectra of galactic cosmic rays for mission STS-61C.

REFERENCES

Adams J.H., Jr., Silberberg R. and Tsao C.H. (1981) Cosmic Ray Effects on Microelectronics, Part I: The Near-Earth Particle Environment, NRL Memorandum Report 4506 (August).

Adams J.H., Jr., Letaw J.R. and Smart D.F. (1983a) Cosmic Ray Effects on Microelectronics, Part II: The Geomagnetic Cutoff Effects, NRL Memorandum Report 5099 (May).

Adams J.H., Jr. (1983b) The variability of single event upset rates in the natural environment, IEEE Trans. Nucl. Sci., NS-30, No. 6.

Adams J.H., Jr. (1986) Cosmic Ray Effects on Microelectronics, Part IV, NRL Memorandum Report 5901 (December).

Allkofer O.C. and Heinrich W. (1974) Attenuation of cosmic ray heavy nuclei fluxes in the upper atmosphere by fragmentation, Nucl. Phys. B71, 429.

Alsmiller R.G., et al. (1974), Photon Spectra from Induced Activity in an Orbiting Spacecraft, ORNL-TM 4345.

Armstrong T.W. and Bishop B.L. (1971) Calculation of the absorbed dose and dose equivalent induced by medium-energy neutrons and protons and comparison with experiment, Rad. Res. 47, 581.

Armstrong T.W., Alsmiller R.G. and Chandler K.C. (1972) Monte Carlo calculations of high energy nucleon-meson cascades and applications to galactic cosmic-ray transport, Proc. Nat. Symp. on Natural and Man-Made Radiation in Space, NASA TM X-2440, 117.

Armstrong T.W., Chandler K.C. and Barish J. (1973) Calculations of neutron flux spectra induced in the Earth's atmosphere by galactic cosmic rays, J. Geophys. Res. 78, 2715.

Armstrong T.W., Colborn B.L. and Watts J.W. (1990) Trapped proton anisotropy, Proceedings Space Station Freedom Ionizing Radiation Working Group Meeting, NASA-MSFC, May 1-3, 1990.

Benton E.V., Frank A.L., Henke R.P., Almasi J.J. and Cassou R.M. (1984) STS-41C Dosimetry Report, USF-TR-64, University of San Francisco.

Benton E.V. and Parnell T.A. (1988) Space radiation dosimetry on U.S. and Soviet manned missions, in: Terrestrial Space Radiation and its Biological Effects, P.E. McCormack, C.E. Swenberg and H. Buecker, eds., NATO ASI Series A, Life Sciences 154, New York, Plenum Press, pp. 729-794.

Berger M. and Seltzer S. (1968) Penetration of Electrons and Associated Bremsstrahlung through Aluminum Targets, Protection Against Space Radiation, National Aeronautics and Space Administration Report, NASA SP-169.

Bertini H.W. (1969) Phys. Rev. 8, 1711.

Bertini H.W., M.P. Guthrie and A.H. Culkowski (1972) Nonelastic Interactions of Nucleons and Pi-Mesons with Complex Nuclei at Energies Below 3 GeV, Oak Ridge National Laboratory ORNL-TM-3148, Oak Ridge, TN.

Bhatt V.L., (1976) Neutron high-energy spectra at 5 mbar near the geomagnetic equator, J. Geophys. Res. 81 (25), 4603.

Binns W.R., Fickle R.K., Garrard T.L., Israel M.H., Klarmann J., Krombel K.E., Stone E.C. and Waddington C.J. (1981) Ap. J. Lett. 247, L115.

Burrell M.O. (1964) The Calculation of Proton Penetration and Dose Rates, Marshall Space Flight Center, NASA TM X-53063.

Cameron A.G.W. (1982) in: Essays in Nuclear Astrophysics, eds. C.A. Barnes, D.D. Clayton and D.N. Schramm, New York: Cambridge University Press, p. 23.

Dudkin V.E. Potapov Yu.V., Akopova A.B., Melkumyan L.V., Benton E.V. and Frank A.L. (1990) Differential neutron energy spectra measured on spacecraft in low Earth orbit, Nucl. Tracks and Rad. Meas. 17 (2), 87-91.

Dyer C.S., et al. (1988) IEEE Trans. Nucl Sci. NS-35 (6), 1401-1411.

Fishman G.J. (1976) Neutron and proton activation measurements from Skylab, Progress in Astronautics and Aeronautics 48, 397-410.

Fishman G.J. and Meegan C.A. (1980) Induced Radioactivity in Recovered Skylab Materials, NASA TM-78263.

Fishman G.J. et al. (1989) Measurement of background radiation on Spacelab 2, Adv. Space Res. 6(4), 23. Also see Paciesas, W.S., Gregory J.C. and Fishman G.J., in AIP Conf. Proc. 186, p. 225.

Fishman G.J., Parnell T.A. and Harmon B.A. (1989) LDEF Induced Radioactivity Analysis Plan, NASA/Marshall Space Flight Center Report (December).

Fowler, J.F. (1981) Nuclear Particles in Cancer Treatment, Bristol: Adam Hilger.

Fowler J.F. (1989) Applications to radiobiology and radiotherapy, Nucl. Tracks and Rad. Meas. 16 (2/3), 89-95.

Frank A.L. and Benton E.V. (1987) Unpublished results.

Greiner D.E., Lindstrom P.J., Heckman H.H., Cork B. and Bieser F.S. (1975) Momentum distributions of isotopes produced by relativistic ^{12}C and ^{16}O projectiles, Phys. Rev. Lett. 35, 152.

Heckman H.H. (1975) Heavy ion fragmentation experiment at the Bevatron, NASA-CR-142589, Washington, D.C.

Heckman H.H. and Nakano G.H. (1969) J. Geophys. Res. 74, 3575.

Heinrich W. (1977) Calculation of LET-spectra of cosmic ray nuclei at various absorber depths, Rad. Eff. 34, 143.

Heinrich W. and Spill A. (1979) Geomagnetic shielding of cosmic rays for different satellite orbits, J. Geophys. Res. 84, 4401.

Heinrich W. (1988) Variation of galactic cosmic radiation by solar modulation, geomagnetic shielding and shielding by matter, in: Terrestrial Space Radiation and its Biological Effects, edited by P.D. McCormack, C.E. Swenberg and H. Buecker, New York: Plenum Press.

ICRU Report No. 16 (1970) International Commission on Radiation Units and Measurements, 4201 Connecticut Ave., NW, Washington, D.C. 20008.

Johnson D.L. and Smith R.E. (1965) The MSFC/J70 Orbital Atmosphere Model and the Data Bases for the MSFC Solar Activity Prediction Technique, NASA TM-86522.

Lenchek A.M. and Singer S.F. (1962) J. Geophys. Res. 67, 4073.

Letaw J.R. (1988) Astronaut Radiation Exposure in Low-Earth Orbit, Part I: Galactic Cosmic Radiation, Severn Communications Co. Report SCC 88-01 (March).

Lindstrom P.J., Greiner D.E., Heckman H.H., Cork B. and F.S. Bieser (1975) Isotope production cross sections for the fragmentation of ^{16}O and ^{12}C at relativistic energies, Lawrence Berkeley Laboratory Report, LBL-3650.

Lockwood J.A., Chen C., Freiling L.A. and St. Onge R.N. (1976) Energy spectrum and flux of high energy neutrons at balloon altitudes, J. Geophys. Res. 81 (34), 6711.

Mathews T. and D. Venkatesan (1990) Unique series of increases in cosmic-ray intensity due to solar flares, Nature 345, 600-602.

Michel R., and Stuck R. (1984) On the production of cosmogenic nuclides in meteoritic material by primary galactic particles, J. Geophys. Res. 89, B637.

Normand E. and Johnson M.L. (1986) ANS Transactions 53, 412-443.

Reedy R.C. and Arnold J.R. (1972) Interaction of solar and galactic cosmic ray particles with the Moon, J. Geophys. Res. 77, 537-555.

Santoro R.T., Claiborne H.C. and Alsmiller R.G., Jr. (1972) Primary and secondary particle contributions to the depth dose distribution in a phantom shielded from solar-flare and Van Allen protons, Proc. Nat. Symp. Natural and Man-Made Radiation in Space, NASA-TM X-2440, 128.

Sawyer D.M. and Vette J.I. (1976) AP8 Trapped Proton Environment for Solar Maximum and Solar Minimum, National Space Science Data Center, Goddard Space Flight Center, NSSDC/WDC-A-R&S 76-06 (June). Also see NASA TM-X-72605 (1976).

Schatten K.H. (1990) The Sun's disturbing behaviour, Nature 345, 578-579.

Shea M.A. and Smart D.F. (1975) Tables of asymptotic directions and vertical cutoff rigidities for a five degree by fifteen degree world grid as calculated using the international geomagnetic reference field for epoch 1975.0, Environ. Res. Pap. 503, AFCRL-TR-0185, Air Force Cambridge Res. Lab, Bedford, Mass.

Silberberg R. and Tsao C.H. (1973) Cross Sections of Proton-Nucleus Interactions at High-Energies, Naval Research Laboratory, NRL 7593, (December).

Silberberg R., Tsao C.H., Adams J.H., Jr. and J.R. Letaw (1984) LET distribution and doses of HZE radiation components at near-earth orbits, Adv. Space Res. 4, 143.

Simpson J.A. (1983) Introduction to the galactic cosmic radiation, in: Composition and Origin of Cosmic Rays, Shapiro, M.M., Ed., Reidel Publishing, Dorcht, Netherlands.

Stassinopoulos E.G. and Mead G.D. (1972) ALLMAG, GDALMG, LINTRA: Computer Programs for Geomagnetic Field and Field-Line Calculations, National Space Science Data Center Report, Goddard Space Flight Center, NSSDC 72-12.

Teague M.J. and Vette J.I. (1974), A Model of the Trapped Electron Population for Solar Minimum, National Science Data Center Report, Goddard Space Flight Center, NSSDC 74-03.

Teague M.J., Chan K.W. and Vette J.I. (1976) AE6: A Model Environment of the Trapped Electrons for Solar Maximum, National Science Data Center Report, Goddard Space Flight Center, NSSDC/WDC-A-R&S 76-04.

Tsao C.H., Silberberg R., Adams J.H., Jr. and Letaw J.R. (1984) Cosmic Ray Effects on Microelectronics, Part III: Propagation of Cosmic Rays in the Atmosphere, NRL Memorandum Report 5402 (August).

Vahia M.N. and Biswas S. (1983) Solar energetic particle studies, in: Composition and Origin of Cosmic Rays, Shapiro, M.M., Ed., Reidel Publishing, Dorcht, Netherlands.

Wagner W. (1987) Report of the Ad Hoc Committee to Review Solar Flare Hazards to Man in Space, Scientific Advisory Board, USAF, Dept. of Air Force (February).

Watts J.W., Jr. and Burrell M.O. (1971) Electron and Bremsstrahlung Penetration and Dose Calculation, National Aeronautics and Space Administration Report, NASA TN D-6385.

Watts J.W., Jr. Parnell T.A. and Heckman H.H. (1989) Approximate angular distribution and spectra for geomagnetically trapped protons in low-earth orbit, High Energy Radiation Background in Space, Proceedings of AIP Conference, Sanibel Island, Florida, V. 186, pp. 75-85, N.Y.

Wefel J.P. (1974) Instrumentation for radiation measurement in space, in: Proceedings of the Workshop on the Radiation Environment of the Satellite Power System (SPS), Schimmerling, W. and Curtis, S.B., Eds., U.S. Dept. of Energy report CONF-7809164, Nat. Technical Information Service, Springfield, VA.

Wefel, J.P. (1988) An overview of cosmic ray research: composition, acceleration and propagation, in: Genesis and Propagation of Cosmic Rays, 1-40, D. Reidel Publishing Company.

Wilson J.W. and Townsend L.W. (1989) Nucleon interaction data bases for background estimates, High Energy Radiation Background in Space, Proceedings of AIP Conference, Sanibel Island, Florida, V. 186, pp. 192-202, N.Y.

Wilson J.W., Townsend L.W. and Khan F. (1989) Evaluation of highly ionizing components in high-energy nuclear radiation fields, Hlth. Phys. 57(5), 717.

ACKNOWLEDGEMENTS

The authors would like to thank W. H. Kinard and J. L. Jones of NASA Langley Research Center, Hampton, VA 23365, for their help and support during this work. The invaluable assistance of V. Rowe of the University of San Francisco with the many aspects of manuscript preparation is also gratefully acknowledged.

CONTRIBUTORS

Tony W. Armstrong
SAIC (location 476)
Route 2
Prospect, TN 38477

Eugene V. Benton
Physics Department
University of San Francisco
San Francisco, CA 94117-1080

James H. Derrickson
ES-62
NASA-Marshall Space Flight Center
Huntsville, AL 35812

Gerald J. Fishman
ES-62
NASA-Marshall Space Flight Center
Huntsville, AL 35812

Allen L. Frank
Physics Research
University of San Francisco
San Francisco, CA 94117-1080

Wolfgang Heinrich
University of Siegen
5900 Siegen
Federal Republic of Germany

Thomas A. Parnell
ES-62
NASA-Marshall Space Flight Center
Huntsville, AL 35812

John W. Watts, Jr.
ES-62
NASA-Marshall Space Flight Center
Huntsville, AL 35812

Burkhard Wiegel
University of Siegen
5900 Siegen
Federal Republic of Germany